Macromolecules

pubs.acs.org/Macromolecules Article

Variation of Spring Stiffness, Monomeric Friction, and Brownian Intensity in the Simulation System of Unentangled Melt under Steady Flow

Nuofei Jiang* and Evelyne van Ruymbeke

Cite This: *Macromolecules* 2023, 56, 2911−2929 Read Online

ACCESS | Metrics & More | Article Recommendations | Supporting Information

ABSTRACT: Understanding the nonlinear dynamics of an unentangled polymer melt from the bead-spring chain model requires knowledge of the variation of spring stiffness, monomeric friction, and Brownian intensity. In this work, these nonequilibrium (NE) parameters are quantified in the model simulation systems of unentangled melt under steady-flow conditions. We focus on a particular version of the model with undefined NE parameters. Some expressions to relate the NE parameters with the rheological and structural properties are pointed out. The spring stiffening parameter r_κ is proven to be easily accessible in the planar flows. The distribution of the stiffening effect along the polymer contour is identified. The alignment-induced reduction of monomeric friction is confirmed in the simulation systems, but the anisotropic feature of friction is also emphasized. The constraint on the cooperative variation of spring stiffness and friction is proven to be an important property of extensional flow. The variation of Brownian intensity is found to be decoupled with the variation of friction, which means the violation of the fluctuation−dissipation (FD) theorem. The NE parameters of the simulation systems are further compared with those from the experimental systems.

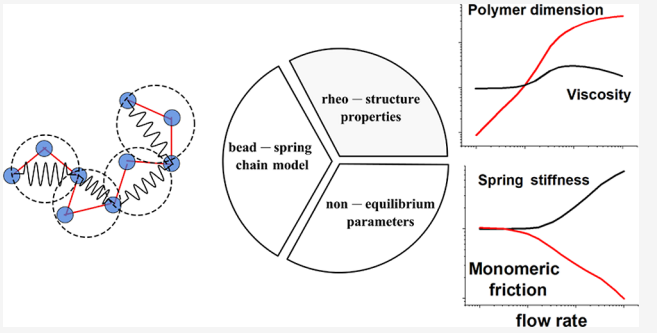

1. INTRODUCTION

It is widely recognized that the bead-spring chain model, also known as the Rouse model, provides a basic framework to understand the dynamics of polymers from the molecular level.[1−3] This model is celebrated for its extreme simplicity and also for the powerful ability to predict the essential dynamic properties in the linear viscoelastic (LVE) regime. With some necessary modifications, it is possible to obtain a quantitative agreement with experimental data from this model. For example, by incorporating a preaveraged hydrodynamic effect, the Zimm model[4] successfully predicts the scaling dependence on the molecular weight of the diffusion constant, rotational relaxation time, and specific viscosity of dilute solution systems. The most amazing part about the Rouse model is that the dynamics of the short polymer melt below a critical molecular weight are well described by this model in its original form. That is, the interchain interaction that causes topological constraint is smoothed out into a mean-field effect in the free-draining limit when the polymers are not strongly overlapped. Although this point has not been fully understood, the Rouse model is always regarded as the starting point in investigating the dynamic phenomena of unentangled polymer melts.

Now that the linear dynamics are well explained by the Rouse model, we would expect that this model can further help us to understand the nonlinear dynamic phenomena in the unentangled melt. However, this is proven to be not so straightforward because the dynamics can be influenced by the variation of nonequilibrium (NE) parameters, including spring stiffness, monomeric friction, as well as the intensity of Brownian force.[5−7] Among these parameters, the variation of spring stiffness is naturally considered because the elasticity of a polymer chain is nonlinear under a large deformation. The spring force between adjacent beads will increase with the elongation and diverge as the bond approaches its maximum before the bond is mechanically degraded. This point has been well understood in the research on the force−extension relationship in polymers.[8] For a freely joined chain, the relationship between elastic force and chain end separation can be analytically expressed as the inverse Langevin function.[9] However, in most cases, the stiffening of spring is described by the finite extensible nonlinear elastic (FENE) law proposed by Warner[10] due to its mathematical simplicity.

The inclusion of nonlinear stiffening of spring has greatly improved the predictions on nonlinear phenomena compared

Received: December 6, 2022
Revised: February 10, 2023
Published: April 4, 2023

Downloaded via UNIV CATHOLIQUE DE LOUVAIN on June 27, 2023 at 08:29:40 (UTC).
See https://pubs.acs.org/sharingguidelines for options on how to legitimately share published articles.

ACS Publications © 2023 American Chemical Society

https://doi.org/10.1021/acs.macromol.2c02458
Macromolecules 2023, 56, 2911−2929

to the original model and is enough to explain some nonlinear phenomena, for example, shear thinning.[11] However, solely incorporating this effect still fails to reach a quantitative description for the rheological data. In particular, in the recent experiments on the extensional rheology of unentangled polystyrene (PS) and poly(*p*-tertbutylstyrene) (PtBS) melts,[12] it has been confirmed that the steady-state extensional viscosity shows thickening followed by thinning as the strain rate increases, while the Rouse model with only the FENE stiffening effect predicts a monotonic thickening. To reach a quantitative agreement, the monomeric friction in this model needs to be considered as a decreasing function of the flow rate. Modification of friction has been suggested by many early works, and many empirical functional forms for nonlinear friction have been proposed.[13−16] For example, in the Giesekus model, the mobility tensor is described as a linear function of the extra stress tensor.[13] Since the friction in the Rouse model represents a mean-field interchain interaction when this model is applied in melt systems, it is considered that the distortion of the surrounding polymers will alter the apparent values of friction. This effect can also be an important factor in the entangled system, especially when comparing the extensional rheology of melt and solution systems with the same LVE profile.[17,18] It is found that the entangled solution system shows a thinning followed by thickening behavior with an extensional rate, while a monotonic thinning is found in the melt system. To explain this feature, in a model used by Ianniruberto,[19] the friction is considered to be a function of the average order parameter combining the ordering of the polymer and solvent molecules. The latter is considered to be always disordered. All these modeling works have proved the fact that including the variation of friction in the original models can always lead to a better description of rheological data. However, the central question, of how should we understand friction from interchain interaction in a predictive manner, remains unclear and is worthy to discuss further.

The Brownian force term is included in the Rouse equation of motion to account for the incessant collision from other molecules. It is expressed as a stochastic force, and the magnitude of its time correlation function is the Brownian intensity. In the equilibrium state, the Brownian force is not seen as an independent factor because its intensity is related to the frictional coefficient based on the fluctuation−dissipation (FD) theorem. Thus, the frictional coefficient alone has already represented all the effects from the surrounding polymers in the Rouse description for melts. However, the validity of the FD theorem in the NE state has been questioned. In addition, some evidence has been raised by Watanabe and his co-workers[7,20] that the Brownian intensity needs to be considered as an independent variable to reach a self-consistent description of the observed properties. For example, the first decay rate of extensional viscosity instantly after the cessation of flow is found to increase with flow rate, which contradicts the prediction based on the validity of the FD theorem. Another piece of evidence arises from their very recent rheo-dielectric experiment of unentangled poly(butylene oxide) (PBO) under shear.[20] Based on the variation of dielectric signals, the authors found that, within the experimental resolution, the flow gradient direction component (yy) of friction decreases with the shear rate, while the Brownian intensity hardly changes upon an increase of the Weissenberg number up to 2. That is, the Brownian and frictional forces are no longer correlated by the FD theorem. These results prove that the Brownian intensity variation is an indispensable factor to describe all these properties in a closed form.

In most cases, the NE parameters are treated as an "input" in the theoretical model to predict the properties observed in an experiment. In fact, their values can also be derived from the known properties so that they become an "output" of the model. Quantifying the features of these NE parameters will enable us to recheck the assumptions involved in the model and identify the key factors that determine their variations. The goal is to build a connection between the coarse-grained mechanical model and the atomistic interactions. In this way, the original model will have more predictive power, and we can get a better understanding of the nonlinear dynamic phenomena from the molecular level. In this work, we plan to quantify the variation of spring stiffness, monomeric friction, and Brownian intensity from the standard molecular dynamics (MD) simulation system of unentangled melt under fast flows. The advantage of working on a simulation system is the accessibility of a large range of properties so that we can use theoretical expressions that involve fewer assumptions. The standard simulation system is based on the classic work by Kremer and Grest (KG).[21] The KG chain system has been intensively investigated by the community, and a full dataset of both rheological properties and microscopic properties is available in both published literature[22−26] and our lab. However, the variation of the NE parameter in this system under the framework of the nonlinear Rouse equation has not been reported yet.

The rest of this work is organized as follows. In Section 2, the details of the NE MD simulation are explained. In Section 3, the basic model equations with undefined NE parameters are introduced. At the beginning of Section 4, the LVE data of the simulation systems are discussed before investigating NE properties. Then, some theoretical expressions that indicate the variation of NE parameters in the steady-flow condition are derived. After that, these expressions are applied to the simulation data of NEMD, and the numerical results of NE parameters are presented. The conditions of extensional and shear flows are discussed separately. To distinguish the two types of flows, the Deborah number (De) will be used for the reduced flow rate of extensional flow, while the Weissenberg number (Wi) is for shear flow. The conclusions of this work are summarized in Section 5.

2. MD SIMULATION

In this section, the details of the simulation systems are explained. In the KG chain system,[21] the pairwise interaction between monomers is the 6−12 Lennard-Jones (LJ) potential truncated and shifted at a cutoff distance of $r_c = 2^{1/6}\sigma_{LJ}$, where σ_{LJ} is the monomer diameter. The energetic parameter is $\epsilon_{LJ} = 1.0\ k_BT$, where k_BT is the reduced energy. The monomers in a polymer chain are connected via the FENE potential: $U_{FENE}(r) = -\frac{kR_0^2}{2}\ln[1 - (r/R_0)^2]$ for $r < R_0$, where $k = 30\ \epsilon_{LJ}/\sigma_{LJ}^2$ and $R_0 = 1.50\ \sigma_{LJ}$. The bending potential is not included. The number density of the monomer is set as $0.85/\sigma_{LJ}^3$. In this work, we will investigate the systems of chain length $N_m = 10$, 20, and 50. Previous studies have suggested that the entanglement length for this chain model is around 68,[27] so the present simulation systems are all in the unentangled regime. Each simulation box contains 400 chains,

https://doi.org/10.1021/acs.macromol.2c02458
Macromolecules 2023, 56, 2911−2929

which is enough to exclude the finite-size effect. All the simulations are performed in the LAMMPS platform.[28]

To apply different types of flows in the simulation system, specific periodic boundary conditions (PBC) need to be used. For shear flow, the Lees−Edwards "sliding brick" PBC is used.[29] The Kraynik−Reinelt (KR) PBC is used to simulate extensional deformation up to a large strain value.[30] The original KR PBC can only be used for planar extension. A later extension of this method has allowed performing uniaxial extension[31,32] by introducing an extra rotational motion for the whole simulation box. The NEMD simulations are performed within the canonical (NVT) ensemble. In the LAMMPS code, the following SLLOD equation of motion together with a Nosé−Hoover thermostat is used for updating MD steps[33,34]

$$\dot{\boldsymbol{r}}_i = \frac{\boldsymbol{p}_i}{m_i} + \boldsymbol{r}_i \cdot \mathbf{K} \tag{1}$$

$$\dot{\boldsymbol{p}}_i = \boldsymbol{F}_i - \boldsymbol{p}_i \cdot \mathbf{K} - \nu^{(\mathrm{NH})} \xi \dot{\boldsymbol{p}}_i \tag{2}$$

$$\dot{\xi} = \nu^{(\mathrm{NH})} \left(\frac{T}{T_0} - 1 \right) \tag{3}$$

where $\mathbf{K}$ is the flow velocity gradient tensor with $K_{ij} = \partial v_i / \partial r_i$. $\boldsymbol{F}_i$ is the total force from the nonbonded and bonded interactions. $\boldsymbol{p}_i$ is the peculiar momentum with respect to the streaming velocity. T is the instant kinetic temperature, and T_0 is the target temperature. $\nu^{(\mathrm{NH})}$ is an adjustable parameter that describes the rate of coupling of particle motion to the heat bath. A recommended value of this parameter is $1/\nu^{(\mathrm{NH})} \approx 100 \times \Delta t$,[28] where $\Delta t = 0.003 - 0.006$ is the timestep of simulation. This choice of $\nu^{(\mathrm{NH})}$ can prevent the temperature of the simulation system from being either too rigid or too unstable. Considering this usage of thermostat in NEMD, the equilibrium MD simulation is also performed under the same thermostat. While a typical KG chain simulation is carried out with a Langevin thermostat.[21] No significant difference is found in the simulation data from the two thermostats, as can be seen from the comparison with a previous simulation study by Likhtman et al.[35] in Figure 3a. In the EMD simulation, the basic LVE properties are collected and the linear relaxation modulus $G(t)$ is measured from the time correlation function of stress based on the Green−Kubo relationship.[36]

The steady-state properties in NEMD are collected from at least three independent simulation runs. The systems are stabilized for a sufficiently long time after the onset of flows to make sure that only the time-independent features are recorded. The reduced viscosity data are presented in Figure 1. These data show the typical features of the experimental systems.[12] Some other rheological and structural data can be found in Section A of the Supporting Information. To prove the validity of these simulation data, we also present direct comparisons with previous NEMD simulation works on the same system[24,25,37,38] in Section B of the Supporting Information. These simulation works have used different thermostats. However, in general, our simulation data agree with them quantitatively, except for some minor differences. Therefore, the simulation data for evaluating NE parameters in the following sections are well validated.

3. THEORETICAL MODEL

The above NEMD simulation data will be investigated from the bead-spring chain equation with undefined NE parameters.

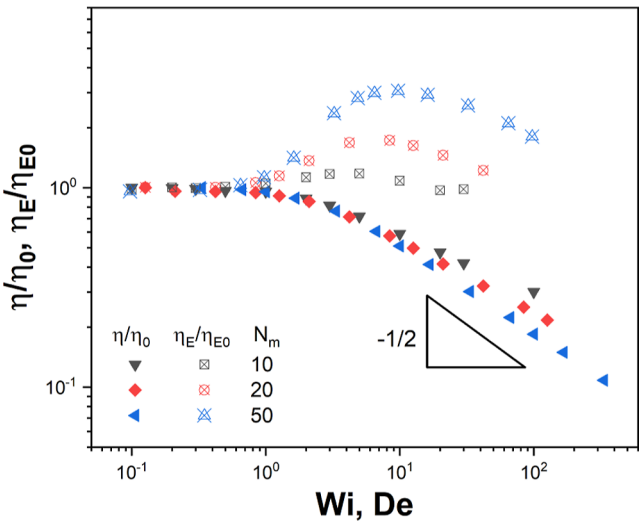

Figure 1. Steady-state values of the reduced shear viscosity and the reduced extensional viscosity under the planar extension of the simulation systems.

The basic model equations will be explained in this section. However, before introducing the model, the standing point of this work needs to be clarified. The mean-field bead-spring chain model is an oversimplification of the complicated multibody interactions in a real polymer melt system. To describe such a system as realistically as possible, the model should have NE parameters that fluctuate locally. However, this type of model can only be investigated via Brownian dynamics (BD) simulation and does not generate analytical expressions. To develop an analytical model, new approximations like decoupling and delocalization (preaveraging along the chain contour) need to be used. For example, in the bead-spring chain models with Warner's FENE spring law, the FENE, FENE-P, and FENE-PM chains are distinguished based on the usage of the approximations,[39] where "P" means the Peterlin approximation.[40] However, solvability always comes with the loss of reality.[41] The systematic errors caused by decoupling and delocalization have been investigated in early studies.[39,42,43] It has been shown that these approximations can lead to pronounced disagreement under time-dependent flows, but they are more acceptable when investigating the steady-state properties. In this work, we wish to make a trade-off between the reality and the solvability of the model. We will focus on the model with decoupled NE parameters to preserve enough solvability. However, the spring coefficient is still treated as a localized quantity (depending on the spring index). This means that the working hypothesis of this model is on the same level as the FENE-P model. It is expected that such a model is closer to the realistic side, compared to the version with an additional delocalization approximation. This point will be discussed in Section 4.2. It is also noteworthy that in the early BD simulation by van den Brule,[39] the spring coefficient is the only NE parameter. Rechecking the systematic errors from decoupling and delocalization when the variations of friction and Brownian intensity are also included in the model, is an important task in our future work.

3.1. Basic Equations of the Model. Based on the above point, we start from the Langevin equation that describes a bead-spring chain ($N + 1$ beads connected by N springs) subject to an arbitrary flow in the following form

https://doi.org/10.1021/acs.macromol.2c02458
Macromolecules 2023, 56, 2911−2929

$$\boldsymbol{\zeta}_n(t)\cdot\left[\frac{\partial \boldsymbol{r}_n(t)}{\partial t} - \mathbf{K}\cdot\boldsymbol{r}_n(t)\right] = -\kappa_0\sum_{m=0}^{N} Z_{nm}\boldsymbol{r}_m(t) + \boldsymbol{F}_{\mathrm{B}n}(t) \tag{4}$$

where $\boldsymbol{r}_n$ (n = 0,1,...,N) is the position of the n th bead. $\boldsymbol{\zeta}_n$ is the frictional coefficient of this bead in the tensor form, which includes the flow-induced anisotropic effect. It is allowed to change with time and flow, without imposing a specific functional form. Under the equilibrium state, $\boldsymbol{\zeta}_n^{(\mathrm{eq})} = \zeta_0\boldsymbol{\delta}$, where $\boldsymbol{\delta}$ is the unit tensor. In the theoretical model, $\boldsymbol{\zeta}_n$ stands for the "effective" friction from atomistic interactions. In the simulation system, the use of a thermostat can impose an "intrinsic" friction due to the coupling with the heat bath. The two concepts need to be distinguished. However, in a dense liquid, the latter is overwhelmed by the former. κ_0 is the equilibrium spring coefficient. Z_{nm} is the element of the connectivity matrix $\mathbf{Z}$ that describes the spring coefficient between the nth and mth segments for $n \neq m$. For linear chains, $\mathbf{Z}$ is a tridiagonal matrix in the form of

$$\mathbf{Z} = \begin{bmatrix} a_0 & -a_0 & & \\ -a_0 & a_0 + a_1 & -a_0 & \\ & & \ddots & \\ & & -a_{N-1} & a_{N-1} \end{bmatrix} \tag{5}$$

where a_n stands for the relative spring coefficient of the bond $\boldsymbol{u}_n = \boldsymbol{r}_{n+1} - \boldsymbol{r}_n$. So, the instance value of the spring coefficient for this bond is $\kappa_0 a_n$. Evidently, $a_n^{(\mathrm{eq})} = 1$ for each n. In the notation of this work, the stiffness of every single bond can change with flow independently. That is to say, the variation of the spring coefficient is included in the whole connectivity matrix and the distribution of stiffness is allowed. $\boldsymbol{F}_{\mathrm{B}n}$ is the Brownian force that represents the random collisions from the surrounding molecules. In a general form, its first- and second-moment averages can be expressed as

$$\langle \boldsymbol{F}_{\mathrm{B}n}(t)\rangle = \mathbf{0}$$
$$\langle \boldsymbol{F}_{\mathrm{B}n}(t)\boldsymbol{F}_{\mathrm{B}m}(t')\rangle = C_1(n-m)C_2(t-t')\mathbf{B}_n \tag{6}$$

where the stochastic nature of Brownian force is retained, but its positional and time correlations are described by the functions C_1 and C_2, respectively. This means the random force could be a "colored" noise. The Brownian force intensity is represented by the tensorial quantity $\mathbf{B}_n$. These expressions under equilibrium are $C_1^{(\mathrm{eq})} = \delta_{mn}$, $C_2^{(\mathrm{eq})} = \delta(t-t')$, and $\mathbf{B}_n^{(\mathrm{eq})} = 2k_BT\zeta_0\boldsymbol{\delta}$.

As explained in the first paragraph of this section, on the most realistic side, all the NE parameters, including $\boldsymbol{\zeta}_n$, a_n, and $\mathbf{B}_n$, should be localized and fluctuating quantities. C_1 and C_2 in the Brownian force could also have finite correlations. For solvability without losing too much reality, the fluctuations in these NE parameters are smoothed out so that they become decoupled quantities. The Brownian force is still described as a "white" noise, which means $C_1 = C_1^{(\mathrm{eq})}$ and $C_2 = C_2^{(\mathrm{eq})}$. The n-dependent nature of spring coefficient variation a_n is retained for discussion because we found that this feature is necessary for explaining the simulation data. However, at the same time, delocalized expressions of $\boldsymbol{\zeta}_n$ and $\mathbf{B}_n$ will be used. The main reason is that we have not found clear evidence that describing the two quantities as n-dependent is necessary. The above approximations are summarized as follows

a_n is replaced by $\langle a_n\rangle$ (7)

$\boldsymbol{\zeta}_n$ is replaced by $\zeta_0\mathbf{r}_\zeta \equiv \frac{1}{N+1}\sum_{n=0}^{N}\langle\boldsymbol{\zeta}_n\rangle$ (8)

$C_1(n-m)C_2(t-t')\mathbf{B}_n$ is replaced by

$$2k_BT\zeta_0\delta_{nm}\delta(t-t')\mathbf{r}_B \equiv \frac{\delta_{nm}\delta(t-t')}{N+1}\sum_{n=0}^{N}\langle\mathbf{B}_n\rangle \tag{9}$$

where $\mathbf{r}_\zeta$ and $\mathbf{r}_B$ are the variations of friction and Brownian intensity in their reduced form. If eq 4 follows the FD theorem, $\mathbf{r}_B = \mathbf{r}_\zeta$. However, $\mathbf{r}_B$ could also decouple from the variation of friction, and then the quantity $\mathbf{r}_B\cdot\mathbf{r}_\zeta^{-1}$ represents the magnitude of the violation of the FD theorem.

More analytical expressions can be generated with the above approximations. Because $\mathbf{Z}$ is a symmetric matrix with its components a_n having real (not imaginary) values, $\mathbf{Z}$ can always be diagonalized, no matter the n dependence of a_n as

$$T^{-1}\mathbf{Z}T = \begin{bmatrix} \theta_0 & & & \\ & \theta_1 & & \\ & & \ddots & \\ & & & \theta_N \end{bmatrix} \tag{10}$$

where θ_p is the eigenvalue of real numbers and $\boldsymbol{T} = [\boldsymbol{v}^0, \boldsymbol{v}^1\cdots, \boldsymbol{v}^N]$ are the eigenvectors of $\mathbf{Z}$. The symmetry of $\mathbf{Z}$ ensures the eigenvectors to satisfy the orthogonal condition

$$\sum_{n=0}^{N} v_n^p v_n^q = I_p\delta_{pq} \tag{11}$$

where

$$I_0 = N+1,\ I_p = \frac{N+1}{2} \qquad \text{for } p = 1,2,\ldots,N \tag{12}$$

This choice of I_p makes v_n^p return to a pure cosine function without a prefactor in the equilibrium state. In a later section, we will show that the enhanced spring coefficient a_n could still be estimated from a specific structural property even if the functional form of a_n is not specified. Based on that, the diagonalization of $\mathbf{Z}$ could then be conducted numerically.

As taking the normal transformation, $\boldsymbol{r}_n$ and $\boldsymbol{F}_{\mathrm{B}n}$ can be rewritten as

$$\boldsymbol{r}_n(t) = \sum_{p=0}^{N}\boldsymbol{\Xi}_p(t)v_n^p(t) \tag{13}$$

$$\boldsymbol{F}_{\mathrm{B}n}(t) = \sum_{p=0}^{N}\boldsymbol{f}_{\mathrm{B}p}(t)v_n^p(t) \tag{14}$$

In the above expression, the eigenvectors also change with time because the functional form of $\mathbf{Z}$ is unknown. Then, the evolution function for the normal coordinate $\boldsymbol{\Xi}_p$ should be written as

$$\zeta_0\mathbf{r}_\zeta(t)\cdot\left[\frac{\partial\boldsymbol{\Xi}_p(t)}{\partial t} + \boldsymbol{\Xi}_p(t)\frac{\partial v_n^p}{v_n^p\partial t} - \boldsymbol{K}\cdot\boldsymbol{\Xi}_p(t)\right] = -\kappa_0\theta_p\boldsymbol{\Xi}_p(t) + \boldsymbol{f}_{\mathrm{B}p}(t) \tag{15}$$

https://doi.org/10.1021/acs.macromol.2c02458
Macromolecules 2023, 56, 2911−2929

In the above expression, the n-dependent time derivative of the eigenvector still exists. This means, in a rigorous sense, a linearized time-evolution function of $\boldsymbol{\Xi}_p$ does not exist if $\mathbf{Z}$ does not follow a fixed form. This issue has been mentioned in the early studies on the FENE-P chain model.[44,45] However, under decoupling approximation, the time derivative term $\partial v_n^p/\partial t$ will vanish in the steady state. After ignoring the second term in the left of eq 15, the dynamic equation for the ensemble-averaged dyadic of the normal coordinate, $\mathbf{A}_p(\equiv\langle\boldsymbol{\Xi}_p\boldsymbol{\Xi}_p\rangle)$ will be in the form of

$$\mathbf{A}_{p(1)} = -\frac{\kappa_0\theta_p}{\zeta_0}\langle\{\boldsymbol{\Xi}_p[\mathbf{r}_\zeta^{-1}\cdot\boldsymbol{\Xi}_p]\} + \{[\mathbf{r}_\zeta^{-1}\cdot\boldsymbol{\Xi}_p]\boldsymbol{\Xi}_p\}\rangle + \frac{2k_BT}{I_p\zeta_0}\{\mathbf{r}_\zeta^{-1}\cdot\mathbf{r}_B\cdot\mathbf{r}_\zeta^{-1}\} \tag{16}$$

where $\mathbf{A}_{p(1)} = \mathrm{d}\mathbf{A}_p/\mathrm{d}t - \mathbf{K}\cdot\mathbf{A}_p - \mathbf{A}_p\cdot\mathbf{K}^T$ is the upper convective time derivative as defined in the textbook.[2] Equation 16 is in a similar form as the expressions used by Watanabe and his co-workers,[6] but more flexibilities are allowed. It is convenient to evaluate the NE parameters as outputs from eq 16, but it is not suitable to use eq 16 as a predictive model because it is not rigorously closed. The procedure to solve the normal coordinate equation in the closed form has been explained by Wiest and Tanner.[45]

The rheological properties are related to the expression of the configurational tensor of the spring unit $\langle\boldsymbol{u}_n\boldsymbol{u}_n\rangle$. After $\mathbf{A}_p$ is solved from eq 16, $\langle\boldsymbol{u}_n\boldsymbol{u}_n\rangle$ will be calculated as

$$\langle\boldsymbol{u}_n\boldsymbol{u}_n\rangle = \sum_{p=1}^{N}\mathbf{A}_p(v_{n+1}^p - v_n^p)^2 \tag{17}$$

The stress tensor $\boldsymbol{\sigma}(t)$ can be expressed as

$$\boldsymbol{\sigma} = c\sum_{n=0}^{N-1}\kappa_0 a_n\langle\boldsymbol{u}_n\boldsymbol{u}_n\rangle = c\kappa_0\sum_{n=0}^{N-1}\sum_{p=1}^{N}\mathbf{A}_p a_n(v_{n+1}^p - v_n^p)^2 = \frac{(N+1)c\kappa_0}{2}\sum_{p=1}^{N}\mathbf{A}_p\theta_p \tag{18}$$

where c is the number density of polymer chains. The third equivalence is then obtained by expanding $\mathbf{Z}\cdot\boldsymbol{v}^p = \theta_p\boldsymbol{v}^p$. At the same time, we can also have the change of structural properties, including the mean-squared radius of gyration tensor $\langle\mathbf{R}_g^2\rangle$ and the end-to-end distance tensor $\langle\mathbf{R}^2\rangle$. Their components are

$$\langle R_{g\alpha\beta}^2\rangle = \frac{1}{N}\sum_{n=0}^{N}\langle[\boldsymbol{r}_n(t) - \boldsymbol{r}_{cm}]_\alpha[\boldsymbol{r}_n(t) - \boldsymbol{r}_{cm}]_\beta\rangle = \frac{1}{2}\sum_{p=1}^{N}A_{p,\alpha\beta} \tag{19}$$

$$\langle R_{\alpha\beta}^2\rangle = \sum_{p=1}^{N}A_{p,\alpha\beta}(v_N^p - v_0^p)^2 = 4\sum_{p=\mathrm{odd}}^{p\le N}A_{p,\alpha\beta}(v_0^p)^2 \tag{20}$$

The second equivalence in eq 20 holds because all the eigenvectors $\boldsymbol{v}^p$ with p equal to an even number are all symmetrical, while the odd number modes are antisymmetrical.

3.2. Comparison with the Dynamic Equation by Bird et al. (1987). It is important to note that a different form of dynamic equation with anisotropic effects has already been proposed by Bird et al. in their textbook,[2] derived from the kinetic theory of distribution function in phase space. In their expression, the Brownian force term is modified because the velocity distribution could also be anisotropic. Although in some cases, the phase-space theory can lead to similar expressions as the Langevin equation method used in this work, they stand for different ways to describe NE flow phenomena.[46] In the distribution function approach, the Brownian force is a deterministic quantity. In addition, this approach has already assumed the validity of the FD theorem as well as a definition of thermodynamic potential $k_BT\ln\psi$, where ψ is the distribution function in the configurational phase. In contrast, the Langevin equation approach is more flexible. Furthermore, the Brownian force in the form of eq 6 only assumes that the interactions from the surrounding polymers on a test chain are seen as a stochastic force, whose intensity will be determined in a self-explaining manner. These points have been discussed by Watanabe and his co-workers recently.[7] In this work, we wish to find a self-consistent description for quantities that can be identified in simulations or experiments, in a polymeric system of specific chemistry, so the flexibility in the Langevin equation approach is more favored.

3.3. Level of Coarse Graining. In the Rouse equation, the number of beads N is explicitly presented in most of the expressions. So, the structure represented by a "bead" and "spring" unit should be clearly defined. In fact, this is a choice, which depends on the CG level. As illustrated in Figure 2a,

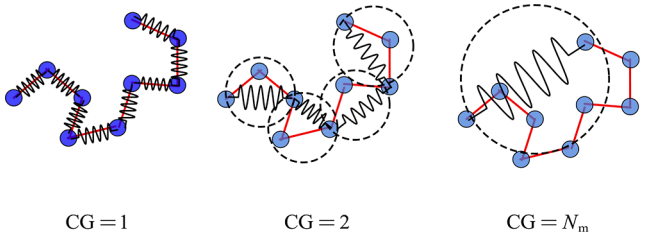

Figure 2. Description of a polymer chain under different CG levels.

"spring" in the Rouse model can represent different numbers of monomer units. The more the polymer is coarse-grained, the more are the units contained in the spring. In the most coarse-grained level, the whole polymer is represented as an elastic dumbbell. In the Rouse equation, the intrachain excluded volume interaction is screened out. As a result, in order to model the K−G chain system properly, the CG level should be larger than the Flory ratio $C_\infty = \langle R^2\rangle/l^2$, where l is the length of the bond, based on the concept of Kuhn segment. For the long-time dynamics under an equilibrium state, the predicted rheological properties, in fact, do not depend on the CG level except for a leftover of the order of $1/N$, which is the idea of dynamic scaling.[1] Indeed, at different CG levels, the spring length and bead friction can be rescaled based on the unvaried polymer dimension and the center-of-mass diffusion constant. In the case of nonlinear flows, it has also been suggested that this scale-insensitive feature should be retained in the variation of NE parameters as long as the polymer is properly coarse-

https://doi.org/10.1021/acs.macromol.2c02458
Macromolecules 2023, 56, 2911−2929

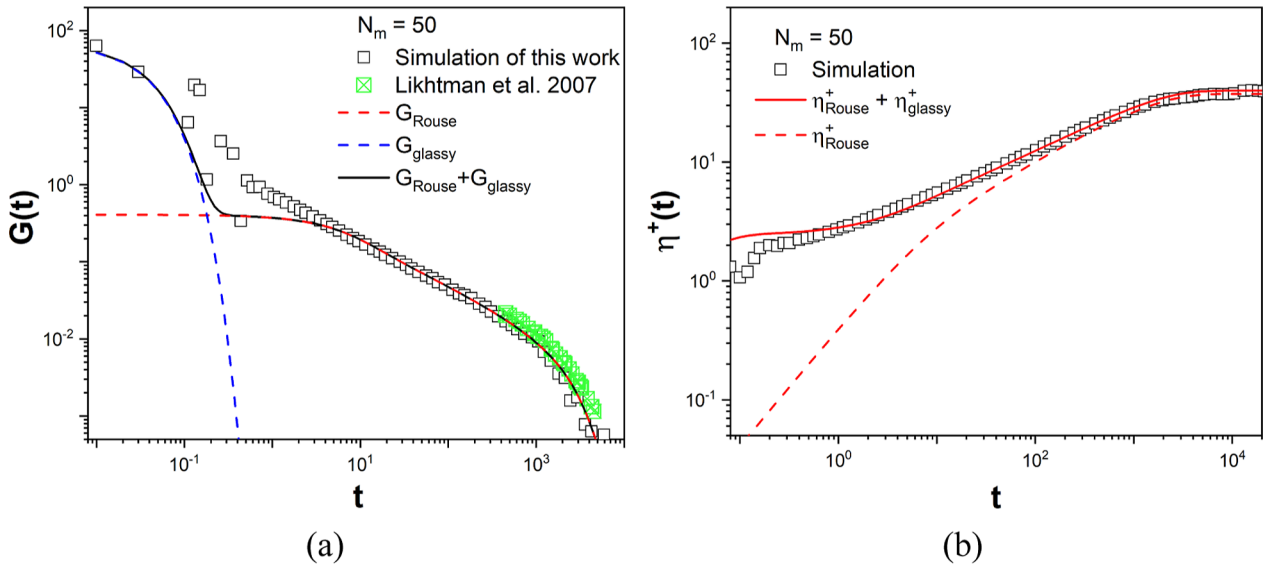

Figure 3. Comparison of the simulation data of the (a) linear relaxation modulus $G(t)$ and (b) linear envelope of viscosity growth function $\eta^+(t)$ with the prediction of the Rouse model, with and without the inclusion of glassy contribution. In (a), the modulus data of the same chain length reported by Likhtman et al.[35] is presented for comparison.

grained.[5] However, to achieve this, both the bead-spring chain and the spring itself should have enough flexibility. Whether or not this argument works in the present simulation system will be checked in a later section. In the simulation systems to be analyzed in this work, the Flory ratio is $C_\infty \approx 1.70$. If not specified, we will work on the level of CG = 2. That is, the spring length will be measured between the second neighboring monomers.

4. RESULTS AND DISCUSSION

4.1. Rouse Model for LVE Properties. Before going into the NE properties, we first checked the predictions of the original Rouse model for LVE properties. In Figure 3, we compare the data for the linear relaxation modulus $G(t)$ and the linear envelope of the viscosity growth function $\eta^+(t)$, which is calculated as $\eta^+(t) = \int_0^t G(t')\mathrm{d}t'$. The LVE function in the simulation system is obtained from the time correlation function of the stress component based on the Green−Kubo relationship, as explained previously. To predict the LVE function from the theoretical model, the equilibrium friction ζ_0 is calculated from the center-of-mass diffusion constant D_{cm}. Based on the Einstein relationship, it should be $\zeta_0 = k_BT/[(N+1)D_{cm}]$. The equilibrium elastic coefficient κ_0 can be estimated from the mean-squared end-to-end distance $\langle R^2\rangle$, that is, $\kappa_0 = 3k_BT/(\langle R^2\rangle/N)$. From the comparison in Figure 3, it can be seen that the long-time relaxation behavior of the simulation system can be well described by the original Rouse model. However, in the short timescales, the prediction is not so satisfying. The inconsistent part is more clearly shown in the transient viscosity function. The reason is that the dynamics below the scale of a spring is not described in the Rouse equation. In order to reach a quantitative agreement with the simulation data, a so-called glassy relaxation mode needs to be included, that is,

$$G(t) = G_{glassy}(t) + G_{Rouse}(t) \tag{21}$$

The necessity to include glassy relaxation has also been confirmed in experimental systems,[47] and it has been found that this mode is more sensitive to the variation of temperature than the Rouse mode. In the work by Iannirubertoet al.,[16] the glassy contribution is also treated separately from the Fraenkel chain modeling. In this work, the glassy relaxation function is described as $G_{glassy}(t) = G(0)\exp(-t/\tau_{glassy})$ ($G_{Rouse}(0)$ is negligibly small compared to $G(0)$). The glassy relaxation time τ_{glassy} is fitted to make the theoretical curve for $\eta^+(t)$ quantitatively agree with simulation data. Using the more flexible KWW function can give a better description of glassy relaxation, but the simple exponential decay expression already works well for our purpose. It is found that $\tau_{glassy} \approx 0.035$ can lead to a good agreement in the three simulation systems with N_m = 10, 20, and 50.

Now that we have identified the existence of the glassy mode in the linear dynamic regime, it is clear that this mode should also contribute to nonlinear rheology but is not described by the nonlinear Rouse model. This contribution is negligible for weak flows, but under fast flow conditions, the glassy mode has a non-negligible effect on the overall stress. As a result, we should define an effective stress that excludes the effect of glassy mode, that is,

$$\sigma_{\alpha\beta}^{(eff)} = \sigma_{\alpha\beta} - \sigma_{\alpha\beta}^{(glassy)} \tag{22}$$

Compared to the Rouse mode, the glassy relaxation time is quite small. In the flow regime we have explored, the glassy mode is well below the onset of nonlinearity ($Wi_{glassy} \leq 0.01$), so its contribution to stress can be calculated from the linear relaxation function. For shear flow, the glassy mode has a finite viscosity $\eta_{glassy} = \int_0^\infty G_{glassy}(t)\mathrm{d}t$. Its contributions to the first and second normal-stress differences are negligibly small. For extensional flow, the contribution of glassy mode to extension viscosity can be obtained from the corresponding Trouton ratio (3 for uniaxial extension and 4 for planar extension). However, compared to shear flow, the influence of glassy mode on extension viscosity is more negligible due to the thickening effect. In the rest of this work, only the effective stress exclusive of glassy mode contribution will be used for calculating NE parameters.

https://doi.org/10.1021/acs.macromol.2c02458
Macromolecules 2023, 56, 2911−2929

4.2. Variation of NE Parameters under Steady Extensional Flow. *4.2.1. Theoretical Expressions under Steady Extensional Flow.* In this section, we quantitatively analyze the variation of spring stiffness, monomeric friction, and Brownian intensity when an unentangled Kremer−Grest melt is subject to steady extensional flows. In this case, the velocity gradient tensor for shear-free extensional flows can be expressed in the form of

$$\mathbf{K} = \begin{bmatrix} \dot{\varepsilon} & 0 & 0 \\ 0 & -m\dot{\varepsilon} & 0 \\ 0 & 0 & (m-1)\dot{\varepsilon} \end{bmatrix} \tag{23}$$

when $m = 1/2$, the flow type is uniaxial extension, while $m = 1$ stands for the planar extension. For convenience, the x component is always set as the extension direction, while the y component is the most contracted direction, so that $m \geq 1/2$. Under pure extensional flows, all the off-diagonal components are zero, so the dynamic equation of eq 16 can be solved easily. The corresponding steady-state solution is

$$A_{p,\alpha\alpha}^{(\mathrm{sf})}(\dot{\varepsilon}) = \frac{2k_BT}{(N+1)\kappa_0\theta_p}\frac{r_{B,xx}}{r_{\zeta,xx}}\frac{1}{1-2\tau_{p,\alpha\alpha}^{*}K_{\alpha\alpha}} \tag{24}$$

where the superscript (sf) represents steady flow. The effective relaxation time $\tau_{p,\alpha\alpha}^{*}$ is defined as

$$\tau_{p,\alpha\alpha}^{*} = \frac{\zeta_0 r_{\zeta,\alpha\alpha}}{2\kappa_0\theta_p} \tag{25}$$

Calculating the observable properties requires summing the contribution from all the eigenmodes. For rheology, the component of stress is

$$\sigma_{\alpha\alpha}^{(\mathrm{sf})} = ck_BT\frac{r_{B,\alpha\alpha}}{r_{\zeta,\alpha\alpha}}[N + Wi_{u\alpha\alpha}^{*}, S\_(Wi_{u\alpha\alpha}^{*}, N, \mathbf{Z})] \tag{26}$$

where the dimensionless quantity $Wi_{u\alpha\alpha}^{*}(= r_{\zeta,\alpha\alpha}\zeta_0 K_{\alpha\alpha}/\kappa_0)$ is a function of frictional variation. The extension component $Wi_{uxx}{}^{*}$ is positive and stands for the effective Weissenberg number of a spring unit with only the variation of friction. The contraction component $Wi_{uyy}{}^{*}$ is negative, and $Wi_{uzz}{}^{*}$ is zero in the case of planar extension.

The notation $S\_$ is the summation terms in the calculation, that is,

$$S\_(x, N, \mathbf{Z}) = \sum_{p=1}^{N}\frac{1}{\theta_p - x} \qquad x < \theta_1 \tag{27}$$

When the connectivity matrix $\mathbf{Z}$ takes the equilibrium form, $S\_$ can be solved analytically but has different forms for a positive and negative value of x. These expressions can be found in the Supporting Information of ref 5. There is an upper limit for the independent variable x in eq 27 when it is used for the extension component because each term of $A_{p,xx}^{(\mathrm{sf})}$ should not be negative due to its physical meaning. In the quasi-linear model where all NE parameters are kept constant, a negative value of $A_{p,xx}^{(\mathrm{sf})}$ simply means the polymer will deform infinitely from the start of flow and there is no steady-state solution for the dynamic equation. Because θ_1 is the smallest eigenvalue, $Wi_{uxx}{}^{*} = \theta_1$ is a critical point for extensional flow. In a realistic system with nonlinear mechanisms, this critical point describes the constraint for the cooperative variation of friction and spring coefficient to reach the steady state. This means the chains decrease their relaxation time under flow in a way that the effective Weissenberg number never exceeds unity.[7] Compared to the extensional component, the solution in the contraction direction does not have such a constraint.

The tensile stress $\sigma_E^{(\mathrm{sf})}$ is expressed as

$$\begin{aligned}\sigma_E^{(\mathrm{sf})} &= \sigma_{xx}^{(\mathrm{sf})} - \sigma_{yy}^{(\mathrm{sf})} \\ &= ck_BT\left[\frac{r_{B,xx}}{r_{\zeta,xx}}Wi_{uxx}^{*}S\_(Wi_{uxx}^{*}, N, \mathbf{Z}) - \frac{r_{B,yy}}{r_{\zeta,yy}}Wi_{uyy}^{*}S\_(Wi_{uyy}^{*}, N, \mathbf{Z})\right] \\ &\quad + cNk_BT\left(\frac{r_{B,xx}}{r_{\zeta,xx}} - \frac{r_{B,yy}}{r_{\zeta,yy}}\right)\end{aligned} \tag{28}$$

Generally, an extra cross-stress $\sigma_C^{(\mathrm{sf})} = \sigma_{zz}^{(\mathrm{sf})} - \sigma_{yy}^{(\mathrm{sf})}$ can also be defined and has a similar expression as $\sigma_E^{(\mathrm{sf})}$.

Then, the reduced extensional viscosity can be expressed as

$$\begin{aligned}\frac{\eta_E}{\eta_{E0}} &= \frac{\sigma_E^{(\mathrm{sf})}/\dot{\varepsilon}}{(2m+2)\eta_0} \\ &= \frac{1}{(m+1)S_0(N, \mathbf{Z}^{(\mathrm{eq})})}\left[r_{B,xx}S\_(Wi_{uxx}^{*}, N, \mathbf{Z}) + mr_{B,yy}S\_(Wi_{uyy}^{*}, N, \mathbf{Z}) + \frac{N\kappa_0}{\dot{\varepsilon}\zeta_0}\left(\frac{r_{B,xx}}{r_{\zeta,xx}} - \frac{r_{B,yy}}{r_{\zeta,yy}}\right)\right]\end{aligned} \tag{29}$$

where η_0 is the zero-shear viscosity. When $m \neq 1/2$, the reduced cross-viscosity is in the form of

$$\begin{aligned}\frac{\eta_C}{\eta_{C0}} &= \frac{\sigma_C^{(\mathrm{sf})}/\dot{\varepsilon}}{(4m-2)\eta_0} \\ &= \frac{1}{(2m-1)S_0(N, \mathbf{Z}^{(\mathrm{eq})})}\left[(m-1)r_{B,zz}S\_(Wi_{uzz}^{*}, N, \mathbf{Z}) + mr_{B,yy}S\_(Wi_{uyy}^{*}, N, \mathbf{Z}) + \frac{N\kappa_0}{\dot{\varepsilon}\zeta_0}\left(\frac{r_{B,zz}}{r_{\zeta,zz}} - \frac{r_{B,yy}}{r_{\zeta,yy}}\right)\right]\end{aligned} \tag{30}$$

The Trouton ratios of η_{E0} and η_{C0} are $(2m+2)$ and $(4m-2)$, respectively.

When it comes to structural properties, the mean-squared radius of gyration and end-to-end distance are in the form of

$$\langle R_{g\alpha\alpha}^2\rangle = \frac{k_BT}{(N+1)\kappa_0}\frac{r_{B,\alpha\alpha}}{r_{\zeta,\alpha\alpha}}S\_(Wi_{u\alpha\alpha}^{*}, N, \mathbf{Z}) \tag{31}$$

$$\langle R_{\alpha\alpha}^2\rangle = \frac{8k_BT}{(N+1)\kappa_0}\frac{r_{B,\alpha\alpha}}{r_{\zeta,\alpha\alpha}}S\_^{(\mathrm{odd},\nu)}(Wi_{u\alpha\alpha}^{*}, N, \mathbf{Z}) \tag{32}$$

where the new summation function $S\_^{(\mathrm{odd},\nu)}$ is defined as

$$S\_^{(\mathrm{odd},\nu)}(x, N, \mathbf{Z}) = \sum_{p=\mathrm{odd}}^{p\leq N}\frac{(v_0^p)^2}{\theta_p - x} \qquad x < \theta_1 \tag{33}$$

https://doi.org/10.1021/acs.macromol.2c02458
Macromolecules 2023, 56, 2911−2929

(a)

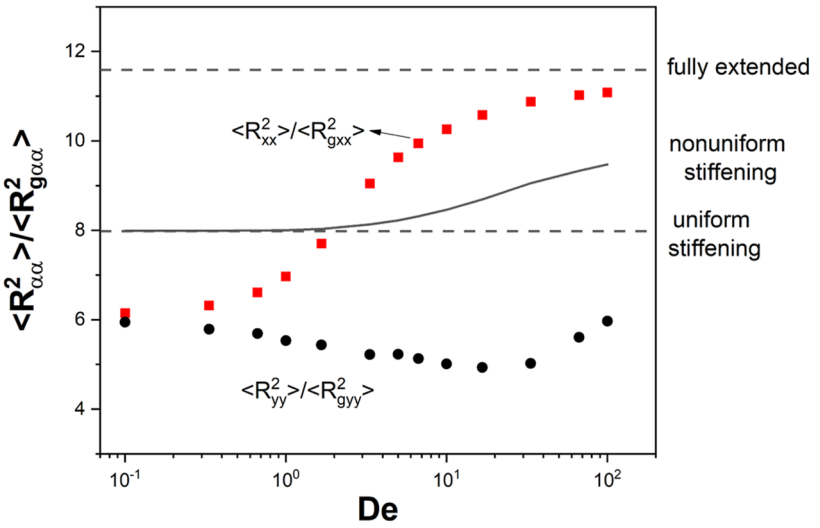

(b)

Figure 4. (a) Value of the structural ratio $\langle R_{\alpha\alpha}^2\rangle/\langle R_{g\alpha\alpha}^2\rangle$ is closely related to the polymer configuration. (b) Scatters stand for the evolution of $\langle R_{xx}^2\rangle/\langle R_{gxx}^2\rangle$ and $\langle R_{yy}^2\rangle/\langle R_{gyy}^2\rangle$ with the flow rate in the NEMD simulation of planar extension. The two horizontal dashed lines stand for the physically permitted maximum value of this structural ratio from the uniform stiffening approximation and the fully extended state. The solid line is obtained from the nonuniform stiffening picture.

Similarly, θ_1 is also the critical point in the function $S_{-}^{(\mathrm{odd},\nu)}$. These polymer dimensions in the reduced form are

$$\lambda_{g\alpha\alpha}^2 = \frac{\langle R_{g\alpha\alpha}^2\rangle}{\langle R_{g\alpha\alpha}^2\rangle_0} = \frac{r_{B,\alpha\alpha}}{r_{\zeta,\alpha\alpha}}\frac{S_{-}(Wi_{u\alpha\alpha}^*, N, \mathbf{Z})}{S_{-}(0, N, \mathbf{Z}^{(\mathrm{eq})})} \tag{34}$$

$$\lambda_{g\alpha\alpha}^2 = \frac{\langle R_{\alpha\alpha}^2\rangle}{\langle R_{\alpha\alpha}^2\rangle_0} = \frac{r_{B,\alpha\alpha}}{r_{\zeta,\alpha\alpha}}\frac{S_{-}^{\mathrm{odd},\nu}(Wi_{u\alpha\alpha}^*, N, \mathbf{Z})}{S_{-}^{\mathrm{odd},\nu}(0, N, \mathbf{Z}^{(\mathrm{eq})})} \tag{35}$$

From these expressions for rheological and structural properties, we can already find some connections between them. Indeed, comparing the expressions of ${\lambda_{g\alpha\alpha}}^2$ with the reduced viscosities, we can rewrite eqs 29 and 30 as

$$\frac{\eta_E}{\eta_{E0}} = \frac{1}{m+1}\lambda_{gxx}^2 r_{\zeta,xx} + \frac{m}{m+1}\lambda_{gyy}^2 r_{\zeta,yy} + \underline{\frac{N\kappa_0}{(m+1)S_{-}(0, N, Z^{(\mathrm{eq})})\dot{e}\zeta_0}\left(\frac{r_{B,xx}}{r_{\zeta,xx}} - \frac{r_{B,yy}}{r_{\zeta,yy}}\right)} \tag{36}$$

$$\frac{\eta_C}{\eta_{C0}} = \frac{m-1}{2m-1}\lambda_{gzz}^2 r_{\zeta,zz} + \frac{m}{2m-1}\lambda_{gyy}^2 r_{\zeta,yy} + \underline{\frac{N\kappa_0}{(2m-1)S_{-}(0, N, \mathbf{Z}^{(\mathrm{eq})})\dot{e}\zeta_0}\left(\frac{r_{B,xx}}{r_{\zeta,xx}} - \frac{r_{B,yy}}{r_{\zeta,yy}}\right)} \quad \text{for } m \neq 1/2 \tag{37}$$

If the violation of the FD theorem is thought to be a trivial factor compared to the variation of polymer dimension and friction, that is, the underlined terms in eqs 36 and 37 are negligibly small compared to the other terms, these expressions can be further simplified. For uniaxial ($m = 1/2$) and planar ($m = 1$) extensions, they are

$$\text{uniaxial extension: } \frac{\eta_E}{\eta_{E0}} \approx \frac{2\lambda_{gxx}^2 r_{\zeta,xx}}{3} + \frac{\lambda_{gyy}^2 r_{\zeta,yy}}{3} \tag{38}$$

$$\text{planar extension: } \frac{\eta_E}{\eta_{E0}} \approx \frac{\lambda_{gxx}^2 r_{\zeta,xx}}{2} + \frac{\lambda_{gyy}^2 r_{\zeta,yy}}{2} \quad \text{(i)}$$

$$\frac{\eta_C}{\eta_{C0}} \approx \lambda_{gyy}^2 r_{\zeta,yy} \quad \text{(ii)} \tag{39}$$

https://doi.org/10.1021/acs.macromol.2c02458
Macromolecules 2023, 56, 2911−2929

This means we can identify the variation of friction from viscosity and radius of gyration without having any knowledge about the stiffening effect. In the above expressions, the two equations for extensional viscosity (eqs 38 and 39) would probably be valid because the polymer deformation in the extensional direction $\lambda_{gxx}{}^2$ will be a large value. In this case, the underlined term in eq 36 will be trivial. On the other hand, the cross-viscosity η_C/η_{C0} and chain deformation $\lambda_{gyy}{}^2$ are both decreasing functions of flow. This means the influence from Brownian intensity variation will probably be non-trivial. Equations 38 and 39 also suggest that it is possible to directly estimate the variation of friction from the experimentally accessible data. The flow-induced anisotropic change of polymer dimension can be measured from the small-angle neutron scattering experiment, as reported by Hassager and co-workers.[48] As long as the measurement is carried out in unentangled samples, the above expression could be directly tested. In addition, the above expressions also suggest that the variation of friction should be independent of the CG level because the bead number N is not explicitly included.

4.2.2. Variation of Nonlinear Parameters with a Uniform Spring Coefficient. The steady-state solutions are more analytically expressed if the stiffness of each spring a_n is assumed to be uniform along the chain. This assumption has been included in the work by Watanabe and his co-workers.[5,6,20,49] This treatment of a_n means another version of the general model

$$a_n \text{ is replaced by } \frac{1}{N+1}\sum_{n=0}^{N}\langle a_n\rangle \tag{40}$$

In this case, the change in the connectivity matrix can be described by a single averaged stiffening parameter, that is, $\mathbf{Z} = r_\kappa \mathbf{Z}^{(eq)}$. The eigenvalues and the eigenvectors of $\mathbf{Z}$ are then analytically expressed as

$$\theta_p(r_k\mathbf{Z}^{(eq)}) = r_\kappa\theta_p^{(eq)} = 4r_\kappa \sin^2\left[\frac{p\pi}{2(N+1)}\right]$$
$$v_n^p(r_k\mathbf{Z}^{(eq)}) = v_n^p(\mathbf{Z}^{(eq)}) = \cos\left[\frac{p\pi(n+1/2)}{N+1}\right] \tag{41}$$

The summation functions used to calculate the rheological and structural properties can also be simplified. That is,

$$S_-(x, N, r_\kappa\mathbf{Z}^{(eq)}) = S_-(x/r_k, N, \mathbf{Z}^{(eq)})/r_k$$
$$S_-^{(odd,\nu)}(x, N, r_\kappa\mathbf{Z}^{(eq)}) = S_-^{(odd,\nu)}(x/r_k, N, \mathbf{Z}^{(eq)})/r_k \tag{42}$$

However, in a further analysis, it is found that this uniform stiffening picture with anisotropic friction is not compatible with our simulation data. We notice this point when we take the ratio of the mean-squared end-to-end distance and the radius of gyration. From their expression in eqs 31 and 32, we have

$$\frac{\langle R_{\alpha\alpha}^2\rangle}{\langle R_{g\alpha\alpha}^2\rangle} = \frac{8S_-^{(odd,\nu)}(Wi_{u\alpha\alpha}^*, N, \mathbf{Z})}{S_-(Wi_{u\alpha\alpha}^*, N, \mathbf{Z})} \tag{43}$$

which is an expression independent of the variation of Brownian intensity. Physically, this ratio $\langle R_{\alpha\alpha}^2\rangle/\langle R_{g\alpha\alpha}^2\rangle$ has a specific link with the configuration of the polymer. As illustrated in Figure 4a, for a flexible polymer under an equilibrium state, this value should be equal to 6. This value is obtained when we set $Wi_{u\alpha\alpha}{}^* = 0$ and $\mathbf{Z} = \mathbf{Z}^{(eq)}$ in eq 43. When the polymer is fully stretched, the configuration will approach the rigid rod limit and $\langle R_{\alpha\alpha}^2\rangle/\langle R_{g\alpha\alpha}^2\rangle$ should be close to 12. If the polymer is more compacted than its equilibrium state, this ratio will be smaller than 6.[50] As a result, under extensional flow, we would expect $\langle R_{xx}^2\rangle/\langle R_{gxx}^2\rangle$ to change from 6 to 12 with the increase of flow rate, while $\langle R_{yy}^2\rangle/\langle R_{gyy}^2\rangle$ would decrease from 6.

When the uniform stiffening approximation is used, the right side of eq 43 is a function of $r_{\zeta,\alpha\alpha}/r_\kappa$, which represents the variation of the effective relaxation time. This means it is possible to obtain $r_{\zeta,\alpha\alpha}/r_\kappa$ by inputting $\langle R_{\alpha\alpha}^2\rangle/\langle R_{g\alpha\alpha}^2\rangle$ into eq 43. However, the variation of $\langle R_{\alpha\alpha}^2\rangle/\langle R_{g\alpha\alpha}^2\rangle$ is limited in some regimes because of the critical point in its expression. The value in the critical point, $\langle R_{\alpha\alpha}^2\rangle/\langle R_{g\alpha\alpha}^2\rangle(Wi_{u\alpha\alpha}^* \to \theta_1)$, is not only a mathematical limit but also stands for the potential a chain can be stretched to if the dynamics of the system are described by our basic equation. Under equilibrium or weak flows, the deformation of the polymer is below this potential because the polymers can still resist the perturbation via their own configurational fluctuation. When the uniform stiffening matrix $\mathbf{Z} = r_\kappa\mathbf{Z}^{(eq)}$ is substituted into eq 43, the upper limit of $\langle R_{\alpha\alpha}^2\rangle/\langle R_{g\alpha\alpha}^2\rangle$ is

$$\max\left(\frac{\langle R_{\alpha\alpha}^2\rangle}{\langle R_{g\alpha\alpha}^2\rangle}\right) = \lim_{x\to\theta_1^{(eq)}}\frac{8S_-^{(odd,\nu)}(x, N, \mathbf{Z}^{(eq)})}{S_-(x, N, \mathbf{Z}^{(eq)})} = 8 \tag{44}$$

The corresponding value is thus smaller than that for the fully extended state. This means the model with uniform stiffening does not allow the appearance of the fully extended state, no matter the rate of extension and the functional forms of the NE parameters. However, when we check this ratio in our simulation system, it is found that the value of $\langle R_{xx}^2\rangle/\langle R_{gxx}^2\rangle$ increases with flow rate and exceeds the value of 8 at only a moderate flow rate. In this case, if the value of $r_{\zeta,xx}/r_\kappa$ is read from eq 43 when $\langle R_{xx}^2\rangle/\langle R_{gxx}^2\rangle > 8$, the limit of the critical point will be violated and a negative value of $A_{p,xx}$ will be found. Except for the extensional component, the variation of $\langle R_{yy}^2\rangle/\langle R_{gyy}^2\rangle$ in the contraction direction shows a nonmonotonic style, which is also unexpected. The inconsistent result regarding $\langle R_{\alpha\alpha}^2\rangle/\langle R_{g\alpha\alpha}^2\rangle$ suggests that a model that assumes a uniform distribution of spring coefficient does not accurately reflect the actual data from simulations and that a more nuanced model, taking into account the variability of stiffness along the polymer contour, is needed.

4.2.3. Variation of NE Parameters with a Nonuniform Spring Coefficient. Now we will discuss the more general case with a nonuniform spring coefficient. Before exploring the behavior under an arbitrary flow rate, we first check the distribution of stiffness in the fully extended state. An important aspect of this fully extended limit is that the steady state of the polymer will be governed by the balance between the elastic force and frictional force. In comparison, the fluctuation due to thermo noise will be a trivial factor. Such an argument was first suggested by Frenkel many years ago[51] and also mentioned by some other researchers afterward.[52−54] In stage III of Figure 5, the nth spring on the left side of the chain needs to balance the frictional force acting on all the beads to

https://doi.org/10.1021/acs.macromol.2c02458
Macromolecules 2023, 56, 2911−2929

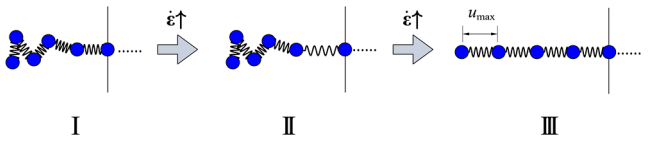

Figure 5. Illustration of polymer configuration under extensional flow. In the linear flow regime of stage I, the springs are not stiffened but only oriented. In stage II with a higher flow rate, the spring closer to the chain center is more elongated and oriented than the outer one. In the fully extended limit of stage III, the orientation is the same along the chain contour, but the distribution of tension is highly nonuniform.

its left. The right half is a symmetric case. In this limit, all the springs have been stretched near the maximum, so the length of each bond is the same. As a result, the tension in the nth spring is written as

$$F_n^{(\mathrm{Elas})} = r_{\zeta,xx}^{(\mathrm{rod})}\zeta_0 u_{\max}\dot{\varepsilon}\sum_{i=0}^{n}\left(\frac{N}{2}-i\right) \qquad \text{for } n < \frac{N}{2} \tag{45}$$

where $r_{\zeta,xx}^{(\mathrm{rod})}$ is the relative friction in this rod limit and $u_{\max}$ is the maximum length of the bond. From eq 45, it can be seen that to maintain the balance in the fully extended state, the inner bond should bear more tension than the outer bonds. According to this distribution of tension, the elements in the connectivity matrix $\mathbf{Z}^{(\mathrm{rod})}$ can now be expressed as

$$a_n^{(\mathrm{rod})} = \frac{r_{\zeta,xx}^{(\mathrm{rod})}\zeta_0\dot{\varepsilon}}{\kappa_0}\begin{cases}\displaystyle\sum_{i=0}^{n}\left(\frac{N}{2}-i\right) & \text{for } n < \frac{N}{2}\\ \displaystyle\sum_{i=0}^{N-n}\left(\frac{N}{2}-i\right) & \text{for } n \geq \frac{N}{2}\end{cases} \tag{46}$$

Based on the above expression, the eigenvalue problem of $\mathbf{Z}^{(\mathrm{rod})}$ can be solved, at least numerically.

Then, we recalculate the maximum of the structural ratio $\langle R_{a\alpha}^2\rangle/\langle R_{g\alpha\alpha}^2\rangle$ by considering $\mathbf{Z}^{(\mathrm{rod})}$ into eq 43 and obtain a value as illustrated in Figure 4. It is found that this value is very close to the rigid rod limit (≈12). This means that this fully extended state under an extremely high extensional rate will be well explained by the current model as long as the stiffness is described by $\mathbf{Z}^{(\mathrm{rod})}$. In our simulation system, this fully extended limit is, in fact, not reached. In a realistic experimental system, chain rupture is usually observed before full stretching. As a result, the situation described by eq 46 is a theoretical limit. However, before this limit, it should be possible to observe the transition from uniform to nonuniform stiffening. Then, including this nonuniform stiffening effect will allow us to discuss the NE parameters in a more realistic model.

To trace the stiffening under arbitrary flow rate, here we suggest to focus on planar extensional flow. Planar extension is more difficult to achieve in the experiment compared to uniaxial extension but easier to be implemented in the simulation. In our simulation systems, it is found that both the extensional stress and the polymer elongation are very close in the two types of extensional flows. Thus, we expect that the variation of the NE parameters should also be similar. For planar extension, the flow is applied only in the xy plane and the zz component is not directly affected. Thus, a simple analytical solution of the zz component can be obtained. That is,

$$A_{p,zz}^{(\mathrm{sf})}(\dot{\varepsilon}) = \frac{2k_BT}{(N+1)\kappa_0\theta_p}\frac{r_{B,zz}}{r_{\zeta,zz}} \tag{47}$$

Then, according to the expression of the spring configurational tensor in eq 17, the length of the nth spring in this direction will be

$$\langle u_{nz}^2\rangle = \langle \boldsymbol{u_n}\boldsymbol{u_n}\rangle_{zz} = \sum_{p=1}^{N} A_{p,zz}^{(\mathrm{sf})}(v_{n+1}^p - v_n^p)^2 = \frac{r_{B,zz}}{r_{\zeta,zz}}\frac{k_BT}{\kappa_0}\frac{1}{a_n} \tag{48}$$

The above expression shows a simple relationship among $\langle u_{nz}^2\rangle$, a_n, and $r_{B,zz}/r_{\zeta,zz}$. In the other words, if the value of $r_{B,zz}/$

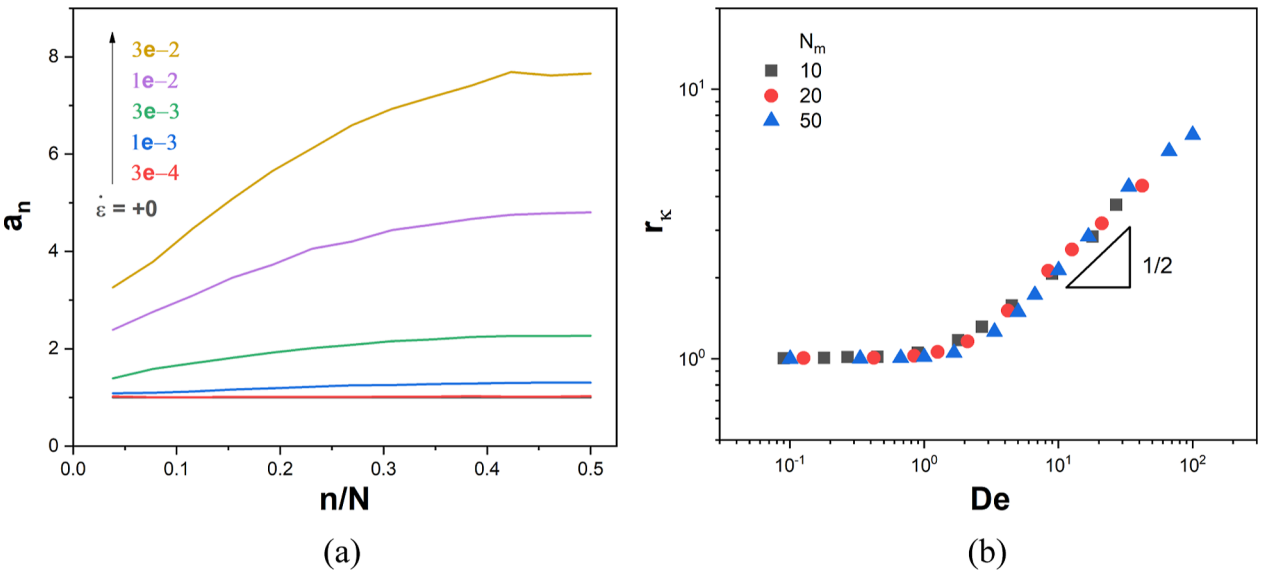

Figure 6. (a) Distribution of spring stiffness under different extensional rates in the simulation system of N_m = 50, derived from the spring length component in the flow-free direction. (b) Variation of the corresponding stiffening parameter r_κ as defined in eq 50.

https://doi.org/10.1021/acs.macromol.2c02458
Macromolecules 2023, 56, 2911−2929

$r_{\zeta,zz}$ has been given and $\langle u_{nz}^2 \rangle$ is characterized in the simulation system, we will have an estimation for the stiffening of individual springs. From a naïve speculation, because the z direction is not interrupted by flow, the FD theorem in this direction could be only violated weakly. That is, $r_{B,zz}/r_{\zeta,zz} \approx 1$. If this assumption is taken, a very simple expression for the stiffening of each spring is obtained, that is,

$$a_n \approx \frac{\langle u_{nz}^2 \rangle_0}{\langle u_{nz}^2 \rangle} \tag{49}$$

The validity of this expression will be checked later. According to the above expression, the spring length distribution in the simulation system is measured under an arbitrary flow rate and then the full information of stiffening is obtained. The corresponding result is shown in Figure 6a. The data show clearly that the spring coefficients grow with the increase in flow rate and the stiffening effect is not uniform along the polymer contour. The relative stiffness in the middle part of the polymer is stronger than the outer springs, which is similar to the case of full extension.

A larger value of the spring coefficient is a natural result of a stronger elongation of the spring. However, the nonuniform elongation does not start from the linear flow regime. In the weak flow regime, the polymer can adjust its configuration with only the effect of reorientation. However, at this stage, the distribution of orientation is not uniform. Similarly, the middle springs will be more oriented. With the increase in flow rate nonlinear stretching will be turned on and coupled with the reorientation effect. This evolution of polymer configuration with the flow rate is illustrated in Figure 4. This picture is consistent with early works on polymer configurations under extensional flow[55,56] and is also supported by the research on the dragging reduction effect of polymer additives. It is found that the polymer chain is always degraded from the middle, even in the transient-flow condition.[57,58] The idea proposed in this section provides a way to understand this phenomenon quantitatively. It should be noted that the model with uniform spring coefficients also suggests a stronger stretch and tension in the chain middle. However, our result shows that a distribution of the spring coefficient could emerge naturally, so it is unnecessary to preaverage this stiffening parameter in our cases.

The eigenvalue problem of $\mathbf{Z}$ is then solved numerically for each set of a_n. We can also redefine the stiffening parameter as the change of the smallest nonzero eigenvalue of the connectivity matrix. That is,

$$r_\kappa \equiv \frac{\theta_1(\mathbf{Z})}{\theta_1(\mathbf{Z}^{(eq)})} \tag{50}$$

The results of r_κ obtained in the simulation systems with different chain lengths are presented in Figure 6b. It can be seen that the data falls into a master curve, and r_κ shows an apparent scaling exponent with the extension rate as $r_\kappa \sim De^{1/2}$. This scaling exponent is determined by the chemistry of the simulation system (LJ pairwise potential and FENE bond potential). However, presently the explicit relationship between the scaling exponent and the force field is not clear. Especially, if the long-chain melt is diluted by some short oligomers, the flow-rate dependence of r_κ should be stronger due to the suppressed friction reduction mechanism. We further quantified the stiffening effect under different CG levels, based on the concept explained in the previous section. From Figure 7, it can be seen that the stiffening parameter indeed depends on the definition of a spring. The more coarse-

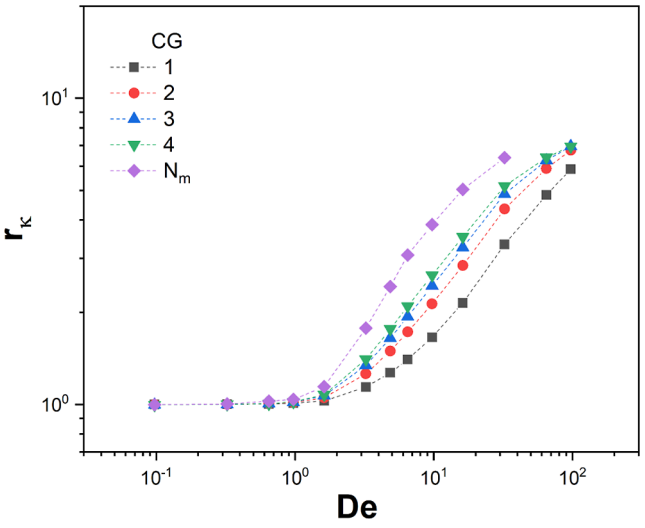

Figure 7. Variation of the stiffening parameter measured from different CG levels in the simulation system of $N_m = 50$.

grained the polymer chain, the larger the value of r_κ observed. At the same time, it is also found that the overall trend of stiffening is very similar and the stiffening parameters are quite close under some CG regimes. This means the scale-insensitive feature does exist in the variation of stiffness, which supports the statement that the Rouse model is physically sound under fast flow.[5]

After all the stiffening factors have been identified, it becomes much easier to find the variations of the rest of the NE parameters. Before that, we first rechecked the inconsistent part related to the structural ratio $\langle R_{\alpha\alpha}^2 \rangle / \langle R_{g\alpha\alpha}^2 \rangle$. After substituting the connectivity matrix $\mathbf{Z}$ determined by $a_n \approx \langle u_{nz}^2 \rangle_0 / \langle u_{nz}^2 \rangle$ into eq 43, we recalculated the maximum allowed value of $\langle R_{\alpha\alpha}^2 \rangle / \langle R_{g\alpha\alpha}^2 \rangle$, as shown in Figure 4. It can be seen that the value of $\max(\langle R_{\alpha\alpha}^2 \rangle / \langle R_{g\alpha\alpha}^2 \rangle)$ obtained from the nonuniform stiffening matrix is no longer a constant but increases with the flow rate after the turn-on of nonlinear flow. Thus, the simulation data is better described, compared to the uniform stiffening picture. However, under fast flows, these values of $\max(\langle R_{\alpha\alpha}^2 \rangle / \langle R_{g\alpha\alpha}^2 \rangle)$ are still smaller than the simulation data of $\langle R_{xx}^2 \rangle / \langle R_{gxx}^2 \rangle$, which means there is still some inconsistency even if the n-dependent feature of a_n is included. The possible reason could be either the basic approximations of the model as explained in eqs 7−9 or the assumption of $r_{B,zz}/r_{\zeta,zz} \approx 1$ used to evaluate a_n.

Although the inconsistency between $\langle R_{\alpha\alpha}{}^2 \rangle$ and $\langle R_{g\alpha\alpha}{}^2 \rangle$ is not fully resolved, the variation of friction and Brownian intensity can still be calculated in a self-explaining manner as long as the two structural properties are not involved simultaneously. Here, the values of $r_{\zeta,xx}$, $r_{\zeta,yy}$, $r_{B,xx}$, and $r_{B,yy}$ are solved from two reduced viscosities (η_E/η_{E0} and η_C/η_{C0}) and two reduced chain dimensions ($\lambda_{Rxx}{}^2$ and $\lambda_{Ryy}{}^2$). The variations of friction in both the extension and contraction directions are presented in Figure 8. The friction of the contraction component $r_{\zeta,yy}$ can be calculated directly from the data of η_C/η_{C0} and λ_{Ryy}^2. These two properties suggest that $r_{\zeta,yy}$

https://doi.org/10.1021/acs.macromol.2c02458
Macromolecules 2023, 56, 2911−2929

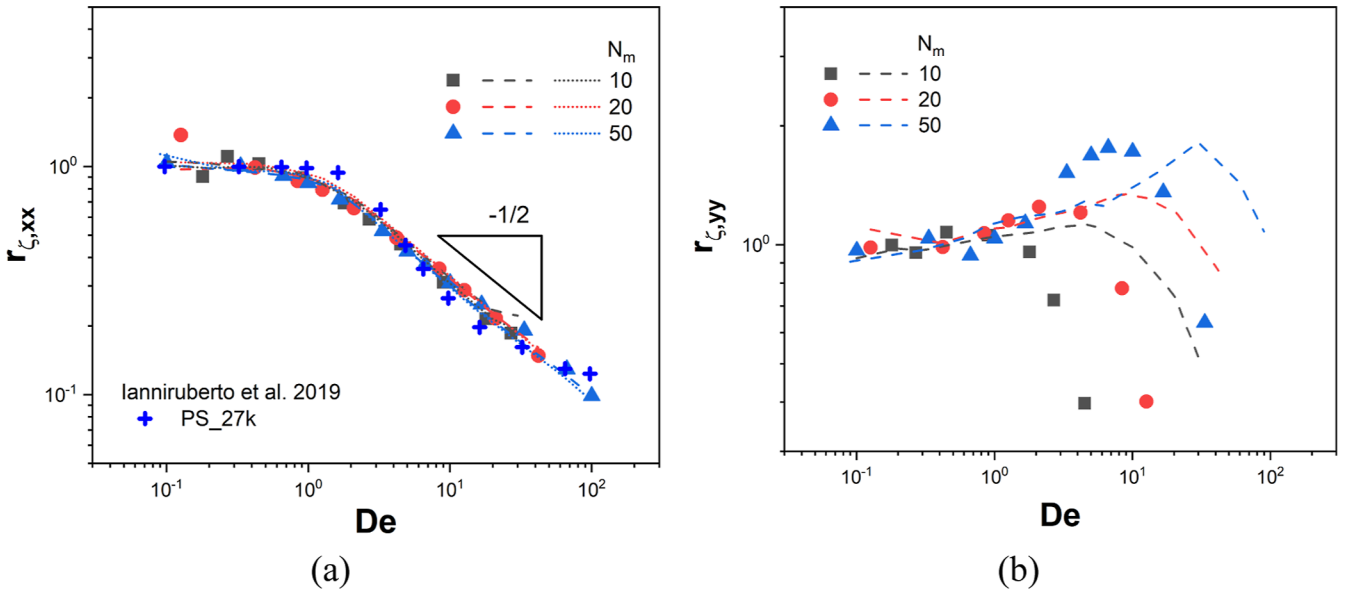

Figure 8. Variation of friction in the (a) extensional and (b) contraction direction. The solid scatters are solved from η_E/η_{E0}, η_C/η_{C0}, λ_{Rxx}^2, λ_{Ryy}^2, and $\langle u_{nz}^2 \rangle$ under planar extension. The dashed lines are estimated from eq 39. The dotted lines are from eq 38, using the simulation data under the uniaxial extensional flow. In (a), the reductions of friction from the order-parameter function for PS proposed by Ianniruberto et al.[16] but using the simulation data as the input are plotted for comparison.

should increase with the flow rate when the flow is not too strong, as shown in Figure 8b. However, this trend of growth does not continue into the strong flow regime. For the friction in the extensional direction, it is found unambiguously that $r_{\zeta,xx}$ is a decreasing function of the flow rate, as presented in Figure 8a. Moreover, similar to the variation of spring stiffness in Figure 6b, the data for simulation systems of different chain lengths can be well shifted into a master curve. The apparent scaling relationship is $r_{\zeta,xx} \sim De^{-1/2}$. We compared these results with the friction obtained from eq 39 that directly relates viscosity, polymer dimension, and friction under planar extension, shown as the dashed lines in Figure 8. It is found that the values of the extensional component $r_{\zeta,xx}$ from two groups of expressions are very close to each other, while for the contraction component $r_{\zeta,yy}$, they agree with each other only in the weak flow regime. Moreover, if we estimate the friction $r_{\zeta,xx}$ under uniaxial extensional flow by ignoring the change of $r_{\zeta,yy}$ in eq 38, the data also agree quite well with planar extension. These results prove that the variation of Brownian intensity is indeed a less important factor in the extension behavior.

The friction reduction data of the simulation systems in Figure 8a are further compared indirectly with those derived from the experimental systems. In the work by Ianniruberto et al.,[16] the extensional rheology data of PS reported by Matsumiya et al.[12] are reproduced by the BD simulation of the Fraenkel chain model. In their BD simulation, the variation of the friction is described by the scalar function: $r_\zeta = [1 + (s/s_c)^2]^{-(n/2)}$, where s is the bond order parameter and $s_c \approx 0.1$ is a critical value for the onset of friction reduction. n is a fitting parameter and fixed to be 1 in one of their later studies.[59] To compare with their data, we measure the values of s in the simulation system under CG = 1 and input them into the above expression for r_ζ. In this indirect comparison with the experimental system in Figure 8a, it is found that the friction reduction data agree quite well. In the previous discussions, it has been explained that the variations of NE parameters are determined by the chemistry of the system and they can also be influenced by the model assumptions. Compared to the bead-spring chain model, the Fraenkel chain model describes the polymeric system from a finer scale and includes the finite extensibility effect implicitly. However, in both the BD simulation by Ianniruberto et al.[16] and the present work, the variations of friction are described as a decoupled and delocalized quantity. In addition, the tensorial feature of friction is not so significant for the extensional flow.[12] In this sense, the agreement found in Figure 8a indicates the fundamental similarity between the KG chain system and PS in their response to the fast flows.

To explain the scaling behavior of $r_{\zeta,xx}$, the variation of the effective relaxation time of the extension component $r_{\zeta,xx}/r_\kappa$ is plotted in Figure 9. Based on the scaling behavior of r_κ and $r_{\zeta,xx}$, clearly, $r_{\zeta,xx}/r_\kappa$ scales with flow rate as $r_{\zeta,xx}/r_\kappa \sim De^{-1}$. This scaling behavior is expected before we calculate r_κ and $r_{\zeta,xx}$

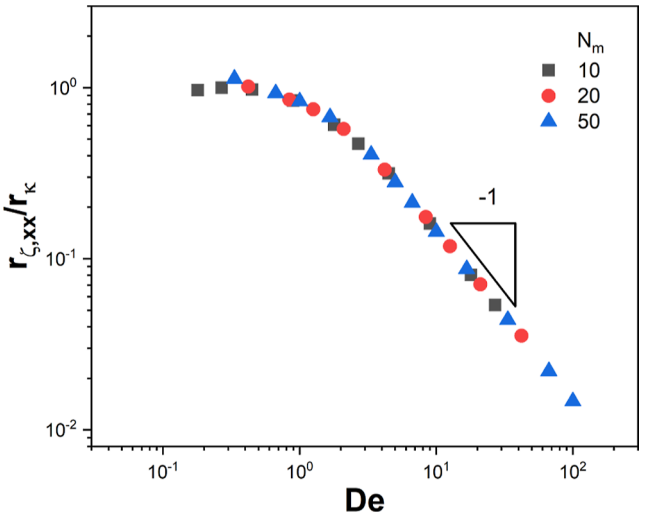

Figure 9. Variation of the effective relaxation time $r_{\zeta,xx}/r_\kappa$ in the extensional direction.

https://doi.org/10.1021/acs.macromol.2c02458
Macromolecules 2023, 56, 2911−2929

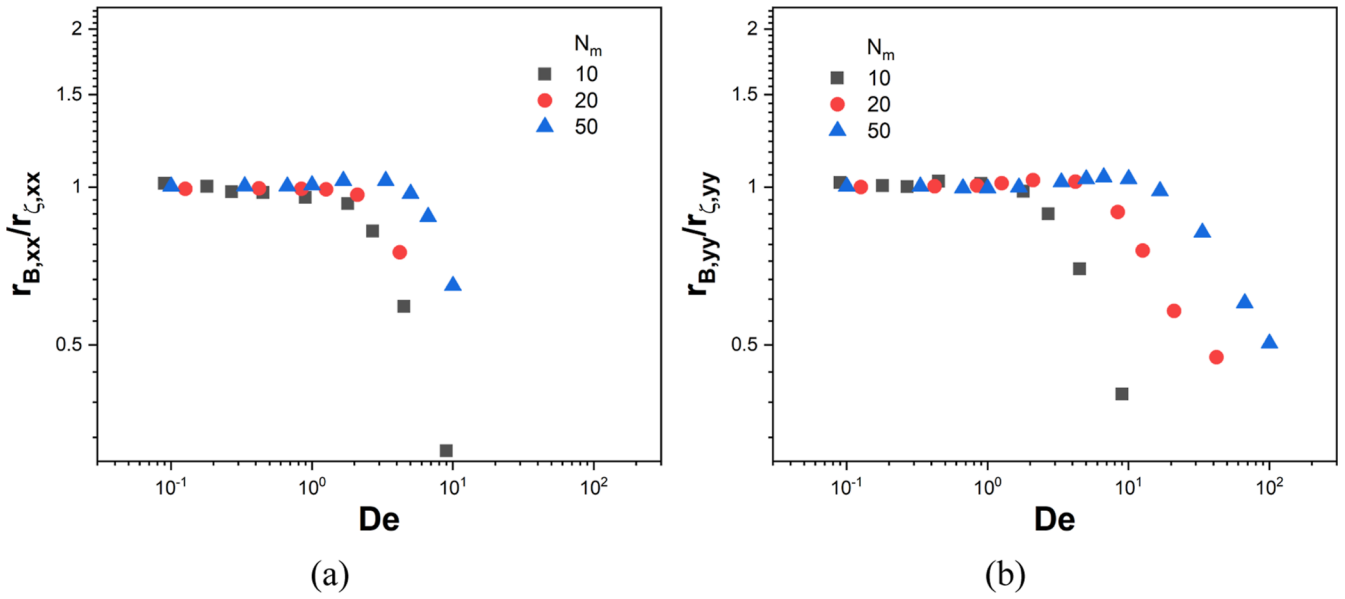

Figure 10. Magnitude of violation from the FD theorem $r_{B,\alpha\alpha}/r_{\zeta,\alpha\alpha}$ in the (a) extensional direction and (b) contraction direction.

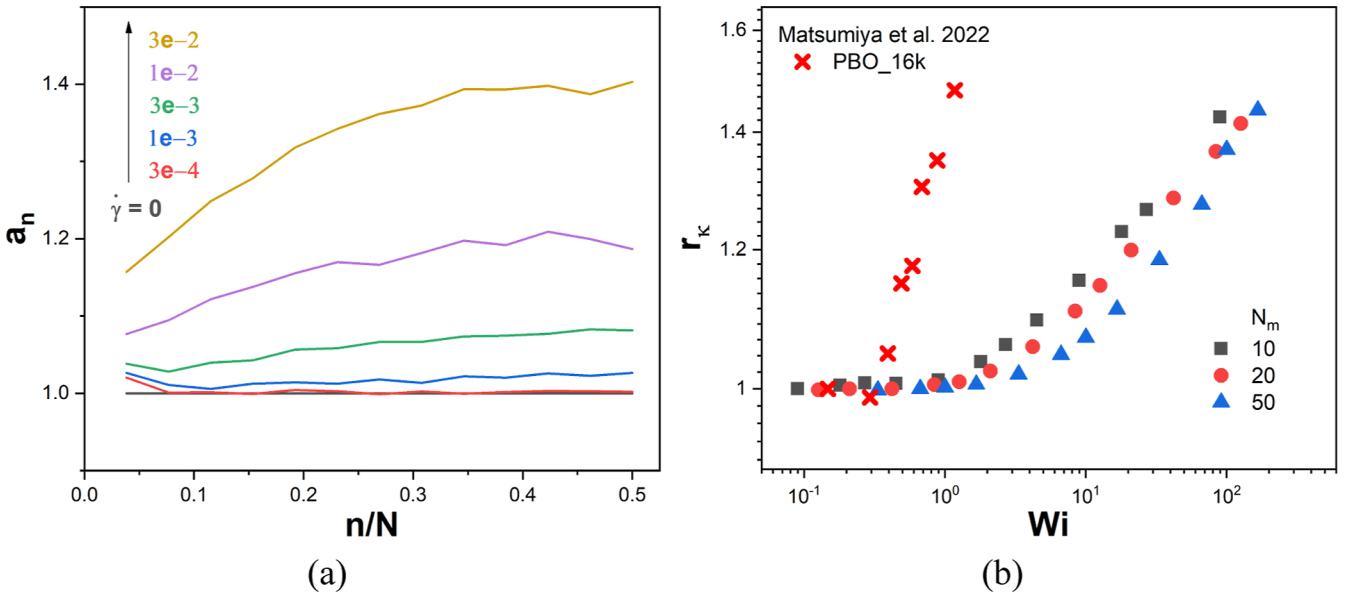

Figure 11. (a) Distribution of spring stiffness under different shear rates in the simulation system of N_m = 50. The presented shear rates are the same as the extensional rate in Figure 6. (b) Variation of the stiffening parameter in simulation systems of different chain lengths. In (b), the r_κ of the PBO sample reported by Matsumiya et al.[20] is presented for comparison.

separately from the rheo-structural properties. Under a fast extensional flow, the polymer chain is fully subjected to the flow, so its effective relaxation $\tau^*_{1,xx}(= r_{\zeta,xx}/r_\kappa\tau_1^{(eq)})$ will be close to the flow characteristic time $1/\dot{\epsilon}$. Mathematically, it means the steady-state solution of $A_{1,xx}$ will always be found near its critical point $Wi_{uxx}{}^* = \theta_1$. A similar argument has been proposed by Watanabe and Matsumiya in the FENE dumbbell model.[60] This characteristic behavior in the extensional flow also provides a cross-check on the stiffening parameter. As explained previously, the frictional variation parameter $r_{\zeta,xx}$ can be derived from eqs 38 or 39 without involving the stiffening parameter, and the apparent scaling exponent is also −1/2. Based on the preassumed variation of effective relaxation time, the stiffening parameter r_κ is supposed to scale with the flow rate as $r_\kappa \sim De^{1/2}$. When deriving the stiffening data in Figure 6, we have assumed no violation of the FD theorem in the flow-free direction, that is, $r_{B,zz}/r_{\zeta,zz} \approx 1$. The consistency between the two independent estimations on r_κ suggests that the related assumption is valid. This proof further explains that the disagreement related to the structural ratio $\langle R^2_{xx}\rangle/\langle R^2_{gxx}\rangle$ should mainly originate from the model assumptions for NE parameters. Considering that $\langle R^2_{xx}\rangle/\langle R^2_{gxx}\rangle$ is a subtle structural property, it is no wonder that the value predicted by the coarse-grained model will be sensitive to the model assumptions.

With the variation of friction, the values of $r_{B,\alpha\alpha}/r_{\zeta,\alpha\alpha}$ can then be derived from the expression of the chain dimension in eq 35. The corresponding result is presented in Figure 10. The result shows that the Brownian intensity is weaker than the friction in both extension and contraction directions, so the

https://doi.org/10.1021/acs.macromol.2c02458
Macromolecules 2023, 56, 2911−2929

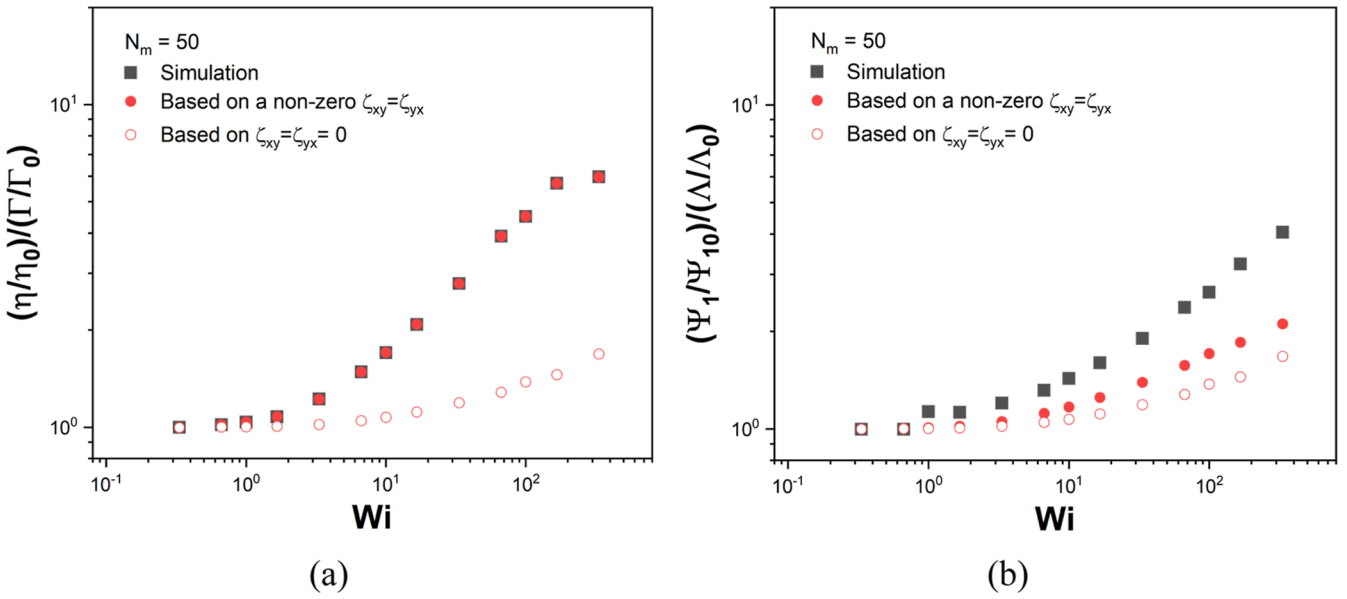

Figure 12. Comparing the simulation result of the function (a) $(\eta/\eta_0)/(\Gamma/\Gamma_0)$ and (b) $(\Psi_1/\Psi_{10})/(\Lambda/\Lambda_0)$ with the predictions with and without nonzero off-diagonal friction.

simulation data indeed suggested the violation of the FD theorem. In addition, this violation does not occur simultaneously in different directions. The variation of $r_{B,xx}/r_{\zeta,xx}$ is found shortly after the onset of nonlinear flow, while for the contraction component, a significant change in $r_{B,yy}/r_{\zeta,yy}$ occurs only in the strong flow regime. The variation of $r_{B,xx}/r_{\zeta,xx}$ under a large flow rate is numerically very sensitive because the involved function is divergent in the critical point. A small fluctuation in the raw data can lead to a significant change in the result. However, this point does not hurt our previous discussions. As it has been demonstrated, the variation of Brownian force will be overwhelmed by the variation of stiffness and friction.

4.3. Variation of the NE Parameter under Steady Shear Flow. In this section, the variation of NE parameters under shear flow will be investigated. In the simple shear flow, the only nonzero element in the flow gradient tensor is $K_{xy} = \dot{\gamma}$. Unlike pure extensional flows, when the dynamic equation of eq 16 is solved for shear flow, the full-form expressions for the solutions will be very complicated if all the off-diagonal components in the friction and Brownian intensity tensors are considered. It indicates that more approximations may be required for the solvability of the model. To identify the variation of NE parameters under shear flow, it has been proposed to incorporate more properties expected for rheological and structural information. For example, Watanabe and his co-workers proposed to measure the in situ dielectric properties of the sample with type-A dipole, in the presence of shear flow, using the facility developed in their lab.[20,49] However, here, since we are working on a simulation system, more structural properties are available, which allows us to highlight some important information. In this section, we still focus on the rheo-structural properties to derive the corresponding NE parameters.

4.3.1. Variation of the Spring Coefficient under Shear Flow. As explained previously, the dynamics in the flow-free direction under any planar flow are only influenced by the stiffening of the spring. Therefore, we can carry out a similar analysis in the sheared system as we did in the planar extension. That is, to evaluate the variation of each spring coefficient from the vorticity (zz) component of spring length according to eq 49. The distribution of spring stiffness under different shear rates is shown in Figure 11a. Meanwhile, the corresponding stiffening parameter r_κ, as defined in eq 50, is shown in Figure 11b. From Figure 11a, it is clear that the shear flow can also result in a nonuniform stiffening effect. That is, the spring closer to the chain center is more stiffened. However, compared to the case of extension of the same flow rate, the stiffening under shear is much weaker and its distribution is also more uniform. This weaker stiffening effect is expected because the polymer is much less elongated, as can be seen from the simulation data in Figure S2 of the Supporting Information. In Figure 11b, the stiffening parameter of the simulation system is further compared with the r_κ of the PBO sample reported by Matsumiya et al.,[20] which is derived from the dielectric loss in the velocity gradient direction ε_y''. Besides, the other NE parameters of the PBO system reported in that study, including the variations of the friction $r_{\zeta,xx}$ and the Brownian intensity $r_{B,yy}$, are also presented in Figures 14 and 15, respectively. According to Figure 11b, the experimental data of PBO show a detectable increase in the spring coefficient at a small Weissenberg number. In contrast, a similar value of r_κ is observed in the simulation system with a much larger Wi. In deriving the NE parameters of the PBO sample, the authors[20] used a similar model as the present work. Thus, the differences in the NE parameters in the weak flow regime should mainly originate from the chemistry of the two systems

4.3.2. Variation of NE Parameters without Off-Diagonal Friction. To identify the NE parameters in the shear plane from rheo-structural properties, we still need the solutions of the dynamic equation. However, the complexity of the solution for shear flow is highly influenced by the off-diagonal component friction. In some works, the off-diagonal friction is assumed to be negligibly small,[61] while there are also some simulation works that suggest that this term could be a non-negligible factor.[62−64] We start from the simpler expressions

https://doi.org/10.1021/acs.macromol.2c02458
Macromolecules 2023, 56, 2911−2929

without off-diagonal friction and check the validity of model prediction. These solutions are

$$A_{p,xy}^{(\mathrm{sf})}(\dot{\gamma}) = \frac{2k_\mathrm{B}T\zeta_0\dot{\gamma}}{(N+1)\kappa_0^2\theta_p^2}\frac{r_{\mathrm{B},yy}r_{\zeta,xx}}{(r_{\zeta,xx}+r_{\zeta,yy})} \tag{51}$$

$$(A_{p,xx}^{(\mathrm{sf})} - A_{p,yy}^{(\mathrm{sf})})(\dot{\gamma}) = \frac{2k_\mathrm{B}T}{(N+1)\kappa_0\theta_p}\left(\frac{r_{\mathrm{B},xx}}{r_{\zeta,xx}} - \frac{r_{\mathrm{B},yy}}{r_{\zeta,yy}}\right) + \frac{2k_\mathrm{B}T\zeta_0^2\dot{\gamma}^2}{(N+1)\kappa_0^3\theta_p^3}\frac{r_{\mathrm{B},yy}r_{\zeta,xx}^2}{(r_{\zeta,xx}+r_{\zeta,yy})} \tag{52}$$

$$(A_{p,yy}^{(\mathrm{sf})} - A_{p,zz}^{(\mathrm{sf})})(\dot{\gamma}) = \frac{2k_\mathrm{B}T}{(N+1)\kappa_0\theta_p}\left(\frac{r_{\mathrm{B},yy}}{r_{\zeta,yy}} - 1\right) \tag{53}$$

where the first term on the right of eq 52 is negligibly small compared to the second term when the bead number N is large enough.[20] To check the validity of these expressions, we can test some predictions from them. For example, based on the form of eq 51, if we define a new structural property as $\Gamma \equiv \langle R_{gxy}^2\rangle/\dot{\gamma}$, which is very similar to the definition of shear viscosity $\eta \equiv \sigma_{xy}/\dot{\gamma}$ but replaces the shear stress by the shear component of the radius of gyration, we will have the following expression

$$\frac{\eta/\eta_0}{\Gamma/\Gamma_0}(\mathbf{Z}) = \frac{\sum 1/(\theta_p^{(\mathrm{eq})})^2}{\sum 1/(\theta_p^{(\mathrm{eq})})}\frac{\sum 1/\theta_p}{\sum 1/\theta_p^2} \tag{54}$$

Similarly, we can also define a structural function based on the solution of the first normal difference as $\Lambda \equiv (\langle R_{gxx}^2\rangle - \langle R_{gyy}^2\rangle)/\dot{\gamma}^2$, which can be compared with the first normal stress coefficient Ψ_1. Then, we will have the following relationship

$$\frac{\Psi_1/\Psi_{10}}{\Lambda/\Lambda_0}(\mathbf{Z}) = \frac{\sum 1/(\theta_p^{(\mathrm{eq})})^3}{\sum 1/(\theta_p^{(\mathrm{eq})})^2}\frac{\sum 1/\theta_p^2}{\sum 1/\theta_p^3} \tag{55}$$

Both eqs 54 and 55 are only functions of spring stiffness, which has been already identified from the vorticity direction. The four rheological and structural properties are all accessible from simulation, so we can directly compare simulation results with the predictions of eqs 54 and 55, as shown in Figure 12. The comparison shows that the prediction is not so satisfying. The predicted values are always smaller than those directly observed in the simulation. A possible solution to fill this gap is to include nonzero off-diagonal components in the frictional tensor, which will be discussed in the following.

4.3.3. Variation of NE Parameters with a Nonzero Off-Diagonal Friction. To proceed with the analysis based on a nonzero off-diagonal friction, we checked the full expression of the solution in the shear plane. Here, we still assume that the friction tensor is symmetrical, that is, $r_{\zeta,xy} = r_{\zeta,yx}$. In the full expressions, it is found that the determinant of the friction tensor, $r_{\zeta,xx}r_{\zeta,yy} - r_{\zeta,xy}{}^2$, appears frequently. We further noticed that the solutions will be analytically trackable if $r_{\zeta,xy}$ is ignored in the determinant but retained in the rest of the expressions. At the same time, the off-diagonal component in the tensor $\{\boldsymbol{r}_\zeta^{-1}\cdot\boldsymbol{r}_\mathrm{B}\}$, which describes the violation of FD theorem, is still set to zero. Such a treatment in the tensorial equation provides more flexibility in the model to describe the simulation data but retains enough solvability at the same time. The corresponding expressions are

$$(A_{p,xy}^{(\mathrm{sf})})(\dot{\gamma}) = \frac{2k_\mathrm{B}T}{(N+1)\kappa_0\theta_p}\frac{\dot{\gamma}r_{\zeta,xx}r_{\mathrm{B},yy}}{(r_{\zeta,xx}+r_{\zeta,yy})(k_0\theta_p/\zeta_0 - \dot{\gamma}r_{\zeta,xy})} \tag{56}$$

$$(A_{p,xx}^{(\mathrm{sf})} - A_{p,yy}^{(\mathrm{sf})})(\dot{\gamma}) = \frac{2k_\mathrm{B}T}{(N+1)\kappa_0\theta_p}\left[\underbrace{\left(\frac{r_{\mathrm{B},xx}}{r_{\zeta,xx}} - \frac{r_{\mathrm{B},yy}}{r_{\zeta,yy}}\right)}_{} + \underbrace{\frac{\dot{\gamma}r_{\zeta,xy}(-r_{\mathrm{B},yy} + r_{\mathrm{B},yy}r_{\zeta,xx}/r_{\zeta,yy} + r_{\mathrm{B},xx} + r_{\zeta,yy}/r_{\zeta,xx})}{(r_{\zeta,xx}/r_{\zeta,yy})(k_0\theta_p/\zeta_0 - \dot{\gamma}r_{\zeta,xy})}}_{} + \frac{\dot{\gamma}^2r_{\zeta,xx}^2r_{\mathrm{B},yy}}{(k_0\theta_p/\zeta_0)(r_{\zeta,xx}+r_{\zeta,yy})(k_0\theta_p/\zeta_0 - \dot{\gamma}r_{\zeta,xy})}\right] \tag{57}$$

$$(A_{p,yy}^{(\mathrm{sf})} - A_{p,zz}^{(\mathrm{sf})})(\dot{\gamma}) = \frac{2k_\mathrm{B}T}{(N+1)\kappa_0\theta_p}\left[\left(\frac{r_{\mathrm{B},yy}}{r_{\zeta,yy}} - 1\right) + \frac{\dot{\gamma}r_{\zeta,xy}r_{\mathrm{B},yy}}{(r_{\zeta,xx}+r_{\zeta,yy})(k_0\theta_p/\zeta_0 - \dot{\gamma}r_{\zeta,xy})}\right] \tag{58}$$

The first two terms on the right of eq 57 are negligibly small compared to the last term, based on a similar argument as eq 52. In case $r_{\zeta,xy}$ is set to zero, eqs 56–58 return to eqs 51–53. Thus, these expressions are more general than those with a zero $r_{\zeta,xy}$. It can also be seen that in all three expressions, the off-diagonal friction appears as the product with the shear rate, that is, $\dot{\gamma}r_{\zeta,xy}$. This means $r_{\zeta,xy}$ needs to be an odd function of the shear rate so that the rheo-structural properties are invariables when the direction of the shear flow is inversed. This is in agreement with the argument explained by Watanabe and his co-workers[20] (Appendix B of their paper).

When the off-diagonal friction is included in the solutions, we can rewrite the functions $(\eta/\eta_0)/(\Gamma/\Gamma_0)$ and $(\Psi_1/\Psi_{10})/(\Lambda/\Lambda_0)$ in the forms of

$$\frac{\eta/\eta_0}{\Gamma/\Gamma_0}(Wi_{uxy}^*, \mathbf{Z}) = \frac{\sum 1/(\theta_p^{(\mathrm{eq})})^2}{\sum 1/\theta_p^{(\mathrm{eq})}}\frac{\sum 1/(\theta_p - Wi_{uxy}^*)}{\sum 1/[\theta_p(\theta_p - Wi_{uxy}^*)]} \tag{59}$$

$$\frac{\Psi_1/\Psi_{10}}{\Lambda/\Lambda_0}(Wi_{uxy}^*, \mathbf{Z}) = \frac{\sum 1/(\theta_p^{(\mathrm{eq})})^3}{\sum 1/(\theta_p^{(\mathrm{eq})})^2}\frac{\sum 1/[\theta_p(\theta_p - Wi_{uxy}^*)]}{\sum 1/[\theta_p^2(\theta_p - Wi_{uxy}^*)]} \tag{60}$$

where $Wi_{uxy}^* = \dot{\gamma}r_{\zeta,xy}\zeta_0/\kappa_0$ is similar to its definition under extensional flow. Compared to the expressions with $r_{\zeta,xy} = 0$ in eqs 54 and 55, the new expressions in eqs 59 and 60 are not only functions of spring stiffness but also the off-diagonal friction. Now that we already have full knowledge about the stiffening matrix $\mathbf{Z}$, it is then possible to identify the values of Wi_{uxy}^* from the simulation result of $(\eta/\eta_0)/(\Gamma/\Gamma_0)$ or $(\Psi_1/\Psi_{10})/(\Lambda/\Lambda_0)$. In Figure 13, we plot the best-fitted values

https://doi.org/10.1021/acs.macromol.2c02458
Macromolecules 2023, 56, 2911−2929

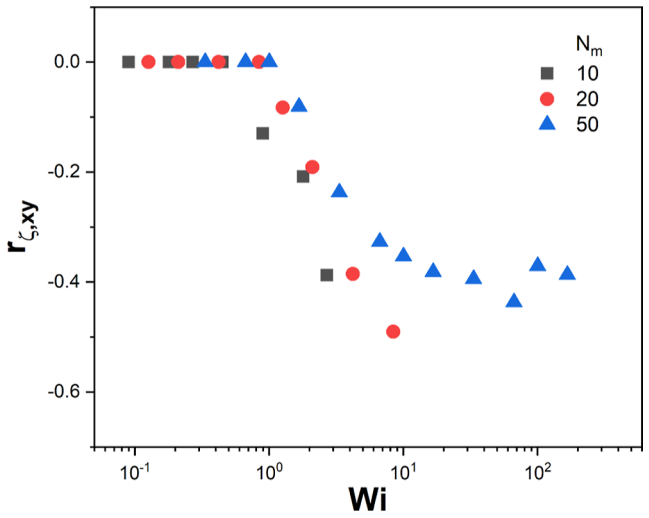

Figure 13. Variation of the off-diagonal friction based on the expression of $(\eta/\eta_0)/(\Gamma/\Gamma_0)$ in eq 59.

of $r_{\zeta,xy}$ for the function $(\eta/\eta_0)/(\Gamma/\Gamma_0)$. The new predictions for the two functions are presented in Figure 12 as solid circles. The result shows that after including a negative value of the off-diagonal friction in eq 59, the simulation data of $(\eta/\eta_0)/(\Gamma/\Gamma_0)$ will be quantitatively explained. When this off-diagonal friction is inputted into eq 60, the new prediction for $(\Psi_1/\Psi_{10})/(\Lambda/\Lambda_0)$ is improved as well. So, the existence of nonzero off-diagonal friction could be the appropriate explanation for the failure of eqs 54 and 55. In the classic definition of friction, a nonzero value of $r_{\zeta,xy}$ is unphysical because it implies a drifting velocity of the whole system. However, in the polymer melt, the change in the atomistic interactions can lead to a nonzero value of $r_{\zeta,xy}$ phenomenally. In addition, the previous NEMD simulation studies[62,65] have suggested that the *xy* component of the diffusivity tensor or the mobility tensor (the inverse of the frictional tensor) under shear flow is positive. The negative $r_{\zeta,xy}$ reported in this work agrees with these studies. It proves that the theoretical expressions in eqs 56−58, which involve additional approximations regarding the off-diagonal elements in the tensorial equations, do not lead to qualitative disagreement. Compared to the nonzero $r_{\zeta,xy}$ in the simulation system, the dielectric data of PBO suggest a negligibly small value of $r_{\zeta,xy}$ because the mode distribution in the dielectric loss ε_y'' is nearly unchanged in the measured range of flows.[20]

For the variation of friction in the flow direction $r_{\zeta,xx}$, we refer to the solutions of the shear component in eq 56 and the first normal difference in eq 57. It is found that the structural function Γ and the first normal-stress difference coefficient Ψ_1 have very similar analytical forms. The ratio of the two functions shows

$$r_{\zeta,xx} = \frac{\Psi_1/\Psi_{10}}{\Gamma/\Gamma_{10}} \tag{61}$$

This expression does not require information on either the spring stiffness or the off-diagonal friction. The corresponding result is shown in Figure 14. It is found that the decrease of Ψ_1 is more significant than Γ, so $r_{\zeta,xx}$ is a decreasing function of the flow rate. Moreover, the simulation data fall into a curve with an apparent scaling exponent of $-1/4$ in the fast flow regime. Based on the experimental data,[20] $r_{\zeta,xx}$ of PBO remains constant in the weak flow regime. A similar comparison of the friction reduction data as Figure 8a is also presented in Figure 14. By inputting the simulation data of the order parameters into the scalar function for PS used by Iannirubertо and Marrucci,[59] it is found that the corresponding magnitude of friction reduction is very close to that from eq 61. However, the previous discussions have suggested the importance to describe friction as a tensorial quantity and the BD simulation by Iannirubertо and Marrucci[59] assumes the validity of the FD theorem. Thus, more evidence is required to explain the semiquantitative agreement in Figure 14.

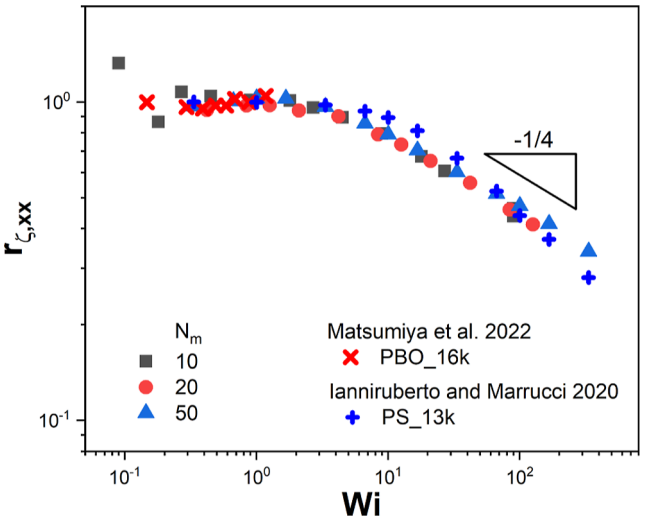

Figure 14. Variation of friction in the shear flow direction $r_{\zeta,xx}$. The corresponding values are derived from eq 61 in the simulation systems, the rheo-dielectric data in the PBO sample,[20] and the order-parameter function for PS used by Iannirubertо and Marrucci.[59]

Equations 56 and 58 further suggest a relationship between the shear stress and the second normal-stress difference. That is,

$$(\sigma_{yy}^{(sf)} - \sigma_{zz}^{(sf)}) - \frac{r_{\zeta,xy}}{r_{\zeta,xx}}\sigma_{xy}^{(sf)} = ck_BT\left(\frac{r_{B,yy}}{r_{\zeta,yy}} - 1\right) \tag{62}$$

Because the frictions $r_{\zeta,xx}$ and $r_{\zeta,xy}$ are already known, the above expression enables us to identify the violation of the FD theorem $r_{B,yy}/r_{\zeta,yy}$ in the flow gradient direction. In addition, eq 62 also explains the two possible origins of the second normal-stress difference: the nonzero off-diagonal friction and the variation of $r_{B,yy}/r_{\zeta,yy}$. By inputting the stress data and the identified frictions into eq 62, it is found that $r_{B,yy}/r_{\zeta,yy}$ decreases from its equilibrium value, as shown in Figure 15. The result shows that both the possible origins contribute to the phenomena of the second normal-stress difference. The decrease of $r_{B,yy}/r_{\zeta,yy}$ with the shear flow rate is similar to what we have found in the extensional flow. However, a different trend is found in the experimental system.[20]

Theoretically, it is possible to find some other NE parameters based on the expressions in eqs 56−58. However, we found it difficult to obtain unambiguous results in further calculations. If the NE parameter is evaluated from an indirect expression, its uncertainty will be amplified and it is more sensitive to the basic model assumptions. Referring to some other measurements other than the pure rheo-structural properties, like the dielectric relaxation as ref 20, would be a

https://doi.org/10.1021/acs.macromol.2c02458
Macromolecules 2023, 56, 2911−2929

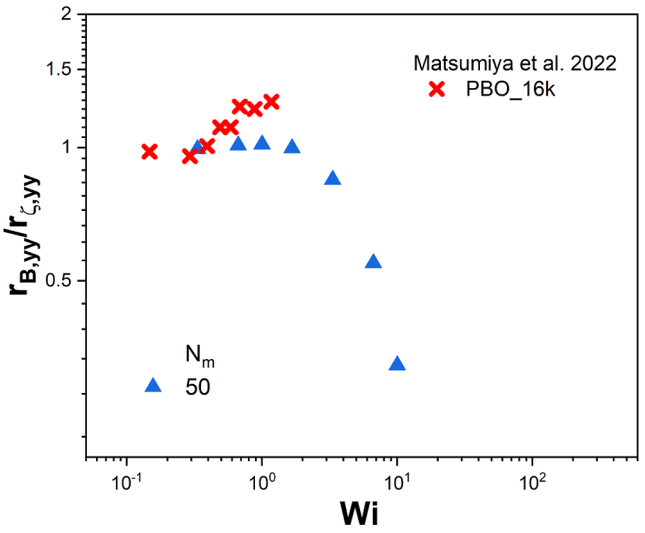

Figure 15. Magnitude of violation from the FD theorem in the flow gradient direction $r_{B,yy}/r_{\zeta,yy}$. It is estimated from eq 62 in the simulation. The experimental data are from Matsumiya et al.[20]

better solution for further discussions. From the experimental side, very recently, it was suggested by Watanabe and his coworkers that measuring the rheological response to the superposed oscillatory strain is also a helpful approach for the study of NE parameters (10.1021/acs.macromol.3c00005).

5. CONCLUSIONS

In this work, we demonstrated how the rheological and structural properties under flow conditions are related via the bead-spring chain model by referring to the NEMD simulation data of the standard chemistry. To do this, the original dynamic equation of the classic Rouse model was modified with all the possible NE factors, including spring stiffness, monomeric friction, and Brownian intensity, but their functional forms were not predefined. We focused on a particular version of the most general model. In this model, solvability is achieved, but the ability to reflect reality is also retained. Based on the theoretical expressions from this model, the variations of NE parameters indicated by the observed rheo-structural data were quantified for both shear and extensional flows. Our result showed that to put these properties into a full picture, variations of all the NE parameters are required. By comparing with other versions of the general model, it was also suggested that some features in the NE parameters of the model are indispensable in explaining some aspects of the real system.

During the analysis, we pointed out that the full information of the spring stiffness can be easily identified if we focus on the planar flows and measure the variation of spring length in the flow-free direction. The following features of the spring stiffening effect are confirmed: (i) the increase of the spring coefficient with the flow rate is not uniform along the polymer contour in both shear and extensional flow and the springs closer to the chain center are more stiffened than the outer ones. This distribution of the spring stiffness is necessary for explaining the transition of the polymer configuration from the random coil to the full stretch; (ii) the stiffening parameter is scale-insensitive in a sound range. For the variation of the monomeric friction, we proposed some simple explicit expressions to evaluate its value. The mechanism of alignment-induced friction reduction was confirmed in our simulation system. The anisotropic feature of the frictional tensor was also emphasized. Especially, the off-diagonal component of the frictional tensor could be a nontrivial factor in relating the rheo-structural properties under the shear flow. To describe the simulation data in a closed form from our current model, we confirmed that the variation of Brownian intensity should be decoupled from friction, which suggests the violation of the FD theorem. It was also suggested that this nonlinear effect is trivial compared to the spring stiffening and the reduction of friction in the extensional deformation of polymer systems. In the comparisons with the experimental systems, it was found that the NE parameters in the simulation systems do not agree with those from PBO quantitatively, but the friction reduction can be well described by the order-parameter function used for the unentangled PS melts.

Although in this work, the NE parameters are quantified only in the simulation system of specific chemistry and this system is not directly linked to any real experimental systems, the theoretical approach can be applied to any other systems. For some simple polymeric systems, like polyethylene, the simulation methods are well developed and the experimental data are well reproduced.[66] Thus, a quick test is easily accessible. Collecting the data of NE parameters from different systems will undoubtedly push forward the understanding of nonlinear flow behaviors.

■ ASSOCIATED CONTENT

Supporting Information

The Supporting Information is available free of charge at https://pubs.acs.org/doi/10.1021/acs.macromol.2c02458.

Some other rheological and structural properties of the simulation systems and direct comparisons of the NEMD simulation data between this work and the previous studies on the same systems (PDF)

■ AUTHOR INFORMATION

Corresponding Author

Nuofei Jiang − *Bio and Soft Matter, Institute on Condensed Matter and Nano-science, Université Catholique de Louvain, Louvain-la-Neuve 1348, Belgium;* orcid.org/0000-0002-6105-354X; Email: nuofei.jiang@uclouvain.be

Author

Evelyne van Ruymbeke − *Bio and Soft Matter, Institute on Condensed Matter and Nano-science, Université Catholique de Louvain, Louvain-la-Neuve 1348, Belgium;* orcid.org/0000-0001-7633-0194

Complete contact information is available at: https://pubs.acs.org/10.1021/acs.macromol.2c02458

Notes

The authors declare no competing financial interest.

■ ACKNOWLEDGMENTS

We deeply acknowledge Hiroshi Watanabe for his critical comments and for sharing the data in ref 20. We also thank Zuowei Wang, Giovanni Ianniruberto, and Giuseppe Marrucci for the fruitful discussion, as well as the anonymous reviewers for their helpful suggestions in improving this article. We thank Zuowei Wang for sharing his unpublished simulation data (the same system as ref 38) for the comparison. N.J. acknowledges

the support from China Scholarship Council (CSC) for his Ph.D. project at UCLouvain. E.V.R. is a research associate of the F.R.S.-FNRS. Computational resources have been provided by the supercomputing facilities of the Université catholique de Louvain (CISM/UCL) and the Consortium des Équipements de Calcul Intensif en Fédération Wallonie Bruxelles (CÉCI) funded by the Fond de la Recherche Scientifique de Belgique (F.R.S.-FNRS) under convention 2.5020.11 and by the Walloon Region.

REFERENCES

(1) Doi, M.; Edwards, S. F. *The Theory of Polymer Dynamics*; Oxford University Press: New York, 1986.
(2) Bird, R. B.; Armstrong, R. C.; Hassager, O. *Kinetic Theory. Dynamics of polymeric liquids*; Wiley, 1987; Vol. *2*.
(3) Rouse, P. E. A theory of the linear viscoelastic properties of dilute solutions of coiling polymers. *J. Chem. Phys.* **1953**, *21*, 1272−1280.
(4) Zimm, B. H. Dynamics of polymer molecules in dilute solution: viscoelasticity, flow birefringence and dielectric loss. *J. Chem. Phys.* **1956**, *24*, 269−278.
(5) Watanabe, H.; Matsumiya, Y.; Sato, T. Revisiting Nonlinear Flow Behavior of Rouse Chain: Roles of FENE, Friction-Reduction, and Brownian Force Intensity Variation. *Macromolecules* **2021**, *54*, 3700−3715.
(6) Sato, T.; Kwon, Y.; Matsumiya, Y.; Watanabe, H. A constitutive equation for Rouse model modified for variations of spring stiffness, bead friction, and Brownian force intensity under flow. *Phys. Fluids* **2021**, *33*, 063106.
(7) Watanabe, H.; Hassager, O.; Matsumiya, Y.; Huang, Q. Extensional Rheology of Unentangled Linear Polymer Melts. In *Recent Advances in Rheology: Theory, Biorheology, Suspension and Interfacial Rheology*; AIP Publishing LLC Melville: New York, 2022. p. 1-1-1-40. DOI: 10.1063/9780735424715_001
(8) Saleh, O. A. Perspective: Single polymer mechanics across the force regimes. *J. Chem. Phys.* **2015**, *142*, 194902.
(9) Treloar, L. G. *The Physics of Rubber Elasticity*; Oxford University Press: London, 1975.
(10) Warner, H. R. Kinetic theory and rheology of dilute suspensions of finitely extendible dumbbells. *Ind. Eng. Chem. Fundam.* **1972**, *11*, 379−387.
(11) Bird, R. B.; Dotson, P. J.; Johnson, N. L. Polymer solution rheology based on a finitely extensible bead-spring chain model. *J. Non-Newtonian Fluid Mech.* **1980**, *7*, 213−235.
(12) Matsumiya, Y.; Watanabe, H.; Masubuchi, Y.; Huang, Q.; Hassager, O. Nonlinear Elongational Rheology of Unentangled Polystyrene and Poly(p-tert-butylstyrene) Melts. *Macromolecules* **2018**, *51*, 9710−9729.
(13) Giesekus, H. A simple constitutive equation for polymer fluids based on the concept of deformation-dependent tensorial mobility. *J. Non-Newtonian Fluid Mech.* **1982**, *11*, 69−109.
(14) Fan, X. J.; Byron Bird, R. B.; Renardy, M. Configuration-dependent friction coefficients and elastic dumbbell rheology. *J. Non-Newtonian Fluid Mech.* **1985**, *18*, 255−272.
(15) Bird, R. B.; Deaguiar, J. R. An encapsulted dumbbell model for concentrated polymer solutions and melts I. Theoretical development and constitutive equation. *J. Non-Newtonian Fluid Mech.* **1983**, *13*, 149−160.
(16) Iannirubertо, G.; Brasiello, A.; Marrucci, G. Modeling Unentangled Polystyrene Melts in Fast Elongational Flows. *Macromolecules* **2019**, *52*, 4610−4616.
(17) Huang, Q.; Hengeller, L.; Alvarez, N. J.; Hassager, O. Bridging the Gap between Polymer Melts and Solutions in Extensional Rheology. *Macromolecules* **2015**, *48*, 4158−4163.
(18) Huang, Q.; Mednova, O.; Rasmussen, H. K.; Alvarez, N. J.; Skov, A. L.; Almdal, K.; Hassager, O. Concentrated Polymer Solutions are Different from Melts: Role of Entanglement Molecular Weight. *Macromolecules* **2013**, *46*, 5026−5035.
(19) Iannirubertо, G. Extensional Flows of Solutions of Entangled Polymers Confirm Reduction of Friction Coefficient. *Macromolecules* **2015**, *48*, 6306−6312.
(20) Matsumiya, Y.; Sato, T.; Chen, Q.; Watanabe, H. Rheo-Dielectric Behavior of Unentangled Poly(butylene oxide) under Steady Shear: Preliminary Evaluation of Non-Equilibrium Parameters at the Onset of Nonlinearity. *Nihon Reoroji Gakkaishi* **2022**, *50*, 371−385.
(21) Kremer, K.; Grest, G. S. Dynamics of entangled linear polymer melts: A molecular-dynamics simulation. *J. Chem. Phys.* **1990**, *92*, 5057−5086.
(22) Daivis, P. J.; Matin, M. L.; Todd, B. D. Nonlinear shear and elongational rheology of model polymer melts at low strain rates. *J. Non-Newtonian Fluid Mech.* **2007**, *147*, 35−44.
(23) Xu, X. L.; Chen, J. Z.; An, L. J. Shear thinning behavior of linear polymer melts under shear flow via nonequilibrium molecular dynamics. *J. Chem. Phys.* **2014**, *140*, 174902.
(24) Xu, X.; Chen, J.; An, L. Probing relationship between structure and viscosity of unentangled polymers in steady shear flow. *Sci. China Chem.* **2017**, *60*, 1609−1616.
(25) Kröger, M.; Hess, S. Rheological evidence for a dynamical crossover in polymer melts via nonequilibrium molecular dynamics. *Phys. Rev. Lett.* **2000**, *85*, 1128−1131.
(26) Kröger, M.; Luap, C.; Muller, R. Polymer Melts under Uniaxial Elongational Flow: Stress−Optical Behavior from Experiments and Nonequilibrium Molecular Dynamics Computer Simulations. *Macromolecules* **1997**, *30*, 526−539.
(27) Everaers, R.; Sukumaran, S. K.; Grest, G. S.; Svaneborg, C.; Sivasubramanian, A.; Kremer, K. Rheology and microscopic topology of entangled polymeric liquids. *Science* **2004**, *303*, 823−826.
(28) Thompson, A. P.; Aktulga, H. M.; Berger, R.; Bolintineanu, D. S.; Brown, W. M.; Crozier, P. S.; in 't Veld, P. J.; Kohlmeyer, A.; Moore, S. G.; Nguyen, T. D.; Shan, R.; Stevens, M. J.; Tranchida, J.; Trott, C.; Plimpton, S. J. LAMMPS - a flexible simulation tool for particle-based materials modeling at the atomic, meso, and continuum scales. *Comput. Phys. Commun.* **2022**, *271*, 108171.
(29) Lees, A. W.; Edwards, S. F. The computer study of transport processes under extreme conditions. *J. Phys. C Solid State Phys.* **1972**, *5*, 1921−1928.
(30) Kraynik, A. M.; Reinelt, D. A. Extensional motions of spatially periodic lattices. *Int. J. Multiphas. Flow* **1992**, *18*, 1045−1059.
(31) Dobson, M. Periodic boundary conditions for long-time nonequilibrium molecular dynamics simulations of incompressible flows. *J. Chem. Phys.* **2014**, *141*, 184103.
(32) Hunt, T. A. Periodic boundary conditions for the simulation of uniaxial extensional flow of arbitrary duration. *Mol. Simul.* **2016**, *42*, 347−352.
(33) Todd, B. D.; Daivis, P. J. *Nonequilibrium Molecular Dynamics: Theory, Algorithms and Applications*; Cambridge University Press, 2017.
(34) Holian, B. L.; Voter, A. F.; Ravelo, R. Thermostatted molecular dynamics: How to avoid the Toda demon hidden in Nosé-Hoover dynamics. *Phys. Rev. E* **1995**, *52*, 2338−2347.
(35) Likhtman, A. E.; Sukumaran, S. K.; Ramirez, J. Linear viscoelasticity from molecular dynamics simulation of entangled polymers. *Macromolecules* **2007**, *40*, 6748−6757.
(36) Morriss, G. P.; Evans, D. J. *Statistical Mechanics of Non-equilbrium Liquids*; Cambridge University Press: Cambridge, 2008.
(37) Kröger, M.; Loose, W.; Hess, S. Rheology and structural changes of polymer melts via nonequilibrium molecular dynamics. *J. Rheol.* **1993**, *37*, 1057−1079.
(38) Amin, D.; Wang, Z. Nonlinear rheology and dynamics of supramolecular polymer networks formed by associative telechelic chains under shear and extensional flows. *J. Rheol.* **2020**, *64*, 581−600.
(39) van den Brule, B. Browian dynamics simulation of finitely extensible bead-spring chains. *J. Non-Newtonian Fluid Mech.* **1993**, *47*, 357−378.

(40) Peterlin, A. Hydrodynamics of macromolecules in a velocity field with longitudinal gradient. *J. Polym. Sci. B Polym. Lett.* **1966**, *4*, 287−291.
(41) Öttinger, H. C. A model of dilute polymer solutions with hydrodynamic interaction and finite extensibility. I. Basic equations and series expansions. *J. Non-Newtonian Fluid Mech.* **1987**, *26*, 207−246.
(42) Herrchen, M.; Öttinger, H. C. A detailed comparison of various FENE dumbbell models. *J. Non-Newtonian Fluid Mech.* **1997**, *68*, 17−42.
(43) Keunings, R. On the Peterlin approximation for finitely extensible dumbbells. *J. Non-Newtonian Fluid Mech.* **1997**, *68*, 85−100.
(44) Wedgewood, L. E.; Ostrov, D. N.; Bird, R. B. A finitely extensible bead-spring chain model for dilute polymer solutions. *J. Non-Newtonian Fluid Mech.* **1991**, *40*, 119−139.
(45) Wiest, J. M.; Tanner, R. I. Rheology of Bead-NonLinear Spring Chain Macromolecules. *J. Rheol.* **1989**, *33*, 281−316.
(46) Bird, R. B.; Ottinger, H. C. Transport properties of polymeric liquids. *Annu. Rev. Phys. Chem.* **1992**, *43*, 371−406.
(47) Inoue, T.; Okamoto, H.; Osaki, K. Birefringence of amorphous polymers. 1. Dynamic measurement on polystyrene. *Macromolecules* **1991**, *24*, 5670−5675.
(48) Hassager, O.; Mortensen, K.; Bach, A.; Almdal, K.; Rasmussen, H. K.; Pyckhout-Hintzen, W. Stress and neutron scattering measurements on linear polymer melts undergoing steady elongational flow. *Rheol. Acta* **2012**, *51*, 385−394.
(49) Sato, T.; Matsumiya, Y.; Watanabe, H. Rheo-Dielectrics and Diffusion of Type-A Rouse Chain under Fast Shear Flow: Method of Evaluation of Non-Equilibrium Parameters for FENE, Friction-Reduction, and Brownian Force Intensity Variation. *Nihon Reoroji Gakkaishi* **2022**, *50*, 253−268.
(50) Rubinstein, M.; Colby, R. H. *Polymer Physics*; Oxford university press: New York, 2003.
(51) Frenkel, J. Orientation and rupture of linear macromolecules in dilute solutions under the influence of viscous flow. *Acta Physicochimica Urss* **1944**, *19*, 51−76.
(52) de Genne, P. G. Coil-stretch transition of dilute flexible polymers under ultrahigh velocity gradients. *J. Chem. Phys.* **1974**, *60*, 5030−5042.
(53) Ianniruberto, G.; Marrucci, G. Molecular Dynamics Reveals a Dramatic Drop of the Friction Coefficient in Fast Flows of Polymer Melts. *Macromolecules* **2020**, *53*, 2627−2633.
(54) Tanner, R. I.; Stehrenberger, W. Stresses in Dilute Solutions of Bead-Nonlinear-Spring Macromolecules. I. Steady Potential and Plane Flows. *J. Chem. Phys.* **1971**, *55*, 1958−1964.
(55) Ryskin, G. Calculation of the effect of polymer additive in a converging flow. *J. Fluid Mech.* **1987**, *178*, 423−440.
(56) Rabin, Y. Polymer conformation in elongational flow. *J. Chem. Phys.* **1988**, *88*, 4014−4017.
(57) Odell, J. A.; Muller, A. J.; Narh, K. A.; Keller, A. Degradation of polymer solutions in extensional flows. *Macromolecules* **1990**, *23*, 3092−3103.
(58) Nguyen, T. Q.; Kausch, H. H. Mechanochemical degradation in transient elongational flow. *Adv. Polym. Sci.* **1992**, *100*, 73−182.
(59) Ianniruberto, G.; Marrucci, G. Origin of Shear Thinning in Unentangled Polystyrene Melts. *Macromolecules* **2020**, *53*, 1338−1345.
(60) Watanabe, H.; Matsumiya, Y. Revisit the Elongational Viscosity of FENE Dumbbell Model. *Nihon Reoroji Gakkaishi* **2017**, *45*, 185−190.
(61) Uneyama, T.; Horio, K.; Watanabe, H. Anisotropic mobility model for polymers under shear and its linear response functions. *Phys. Rev. E* **2011**, *83*, 061802.
(62) Hunt, T. A.; Todd, B. D. Diffusion of linear polymer melts in shear and extensional flows. *J. Chem. Phys.* **2009**, *131*(). DOI: 10.1063/1.3202868
(63) Ilg, P. Thermodynamically consistent coarse graining the non-equilibrium dynamics of unentangled polymer melts. *J. Non-Newtonian Fluid Mech.* **2010**, *165*, 973−979.
(64) Ilg, P.; Kröger, M. Molecularly derived constitutive equation for low-molecular polymer melts from thermodynamically guided simulation. *J. Rheol.* **2011**, *55*, 69−93.
(65) Ianniruberto, G.; Brasiello, A.; Marrucci, G. Simulations of Fast Shear Flows of PS Oligomers Confirm Monomeric Friction Reduction in Fast Elongational Flows of Monodisperse PS Melts As Indicated by Rheooptical Data. *Macromolecules* **2012**, *45*, 8058−8066.
(66) Edwards, B. J.; Nafar Sefiddashti, M. H.; Khomami, B. Atomistic simulation of shear flow of linear alkane and polyethylene liquids: A 50-year retrospective. *J. Rheol.* **2022**, *66*, 415−489.

Recommended by ACS

Rouse Analysis of Nonlinear Rheology of Unentangled Polymer Melts under Fast Shear: Viscoelastic Response to Superposed Oscillatory Strain
Yumi Matsumiya, Hiroshi Watanabe, *et al.*
MARCH 28, 2023
MACROMOLECULES
READ

Nature of Steady-State Fast Flow in Entangled Polymer Melts: Chain Stretching, Shear Thinning, and Viscosity Scaling
Zipeng Xu, Shiwang Cheng, *et al.*
NOVEMBER 22, 2022
MACROMOLECULES
READ

Molecular Dynamics Study on the Validity of Miller–Macosko Theory for Entanglement and Crosslink Contributions to the Elastic Modulus of End-Linked Polym...
Andrei A. Gusev and Fabian Schwarz
SEPTEMBER 12, 2022
MACROMOLECULES
READ

Nonlinear Extensional Rheology of Poly(*n*-alkyl methacrylate) Melts with a Fixed Number of Kuhn Segments and Entanglements per Chain
Shilong Wu, Quan Chen, *et al.*
MARCH 22, 2022
ACS MACRO LETTERS
READ

Get More Suggestions >